Helimagnets by disorder: Its role on the high-temperature magnetic spiral in the YBaCuFeO$_5$ perovskite

Arnau Romaguera ,[1] Xiaodong Zhang ,[1] Oscar Fabelo ,[2] Francois Fauth ,[3]
Javier Blasco ,[4] and José Luis García-Muñoz [1,*]

[1]*Institut de Ciència de Materials de Barcelona, ICMAB-CSIC, Campus UAB, 08193 Bellaterra, Catalunya, Spain*
[2]*Institut Laue-Langevin, 38042 Grenoble, France*
[3]*CELLS-ALBA Synchrotron, 08290 Cerdanyola del Vallès, Barcelona, Spain*
[4]*Instituto de Nanociencia y Materiales de Aragón, Departamento de Física de la Materia Condensada,
CSIC-Universidad de Zaragoza, 50009 Zaragoza, Spain*

Most of the spiral magnetoelectric multiferroics investigated in recent years are geometrically or exchange-frustrated magnets, where the presence of triangular or other frustrated spin networks produce low magnetic transition temperatures. This critically limits their potential uses. The exceptional stability of the spiral magnetic order (at T_S) in the layered structure of the YBaCuFeO$_5$ double perovskite involves a nonconventional mechanism: spiral order by disorder. The model has been theoretically developed by Scaramucci *et al.* [Phys. Rev. Res. **2**, 013273 (2020)] after the discovery of a huge impact of cation disorder on T_S [M. Morin *et al.*, Nat. Commun. **7**, 13758 (2016)]. In this work the influence of disorder (and only disorder) on the magnetic phase diagram is studied on a quantitative basis extending the range of previous studies. We thoroughly investigate the impact of frustration due to B-site disorder (n_d) on the magnetic spirals in the reference composition YBaCuFeO$_5$. The interplay between disorder, stability, and the detailed features of the incommensurate spiral magnetic orders were systematic, quantitative, and methodically investigated in samples of identical composition, spanning a wide range of n_d values. Three different regimes are distinguished in the YBaCuFeO$_5$ phase diagram versus disorder. A triple point is found in YBaCuFeO$_5$ driven by Fe/Cu disorder that sets limits to T_S and the cycloidal component of the helicoidal order. These layered materials appear as a very efficient realization of the avenue "spiral order by disorder" to supply functional helimagnets at normal working temperatures.

I. INTRODUCTION

Research on frustrated materials is receiving continued interest. The inability to satisfy all interactions is at the origin of attractive phenomena and plays important roles in many different systems: classical and quantum magnets, metals, superconductors, multiferroics, dielectrics, etc. In many relevant materials frustration is the cause of gigantic responses, exotic orders, new thermodynamic states, or exceptional dynamics. The materials presenting magnetic chirality form a rare class of frustrated compounds that attract a great deal of attention owing to their unique technologically important properties. These include magnetoelectric coupling, spin-polarized currents, anomalous Hall effect, spin torque phenomena, etc. Noncollinear spin textures with magnetic chirality can occur in chiral crystallographic lattices [1], but also in centrosymmetric nonchiral crystal lattices [2].

Among the appealing properties realized in frustrated magnetic systems the multiferroicity and the magnetoelectricity are two of the most attractive. Most of the spiral magnetoelectric multiferroics investigated in recent years are geometrically frustrated magnets, where the spin-orbit coupling induces ferroelectric polarization in the noncollinear phase through the Dzyaloshinskii-Moriya (DM) interaction. Although spin and ferroelectric orders are coupled "by construction" in such spin-driven multiferroics, their main drawback is that the presence of triangular or more complex frustrated spin networks produces low magnetic transition temperatures for the emergence of the spiral phase at T_S (typically $T_S < 50$ K and at most T_S does not exceed 100 K [3,4]). This critically limits their potential uses in spintronic and low-power magnetoelectric devices.

Exceptionally, the layered perovskites RBaCuFeO$_5$ have been reported to display spiral magnetic order at unexpectedly high temperatures [5–9]. They are considered excellent candidates for cycloidal helimagnets, potentially magnetoelectric, able to retain a configuration of rotating spins up to unusually high temperatures. In the structure of the YBaCuFeO$_5$ (YBCFO) double-perovskite A^{3+}/A^{2+} layers alternate along the c axis ($A^{3+} = $ Y^{3+} or R^{3+} [rare earth] and $A^{2+} = $ Ba^{2+}). B-site metals form CuFeO$_9$ bilayers of corner-sharing Cu^{2+}O$_5$ and Fe^{3+}O$_5$ square pyramids that extend parallel to the ab plane, separated by Y^{3+} (or R^{3+}) layers. The Ba^{2+} ions are

located within the bilayer spacing. There are two nonequivalent sites for B atoms. In a formal ordered sample, Cu atoms are located at $(1/2, 1/2, z \approx 3/4)$, while Fe atoms are placed at $(1/2, 1/2, z \approx 1/4)$ position. *B*-site ordering (Cu^{2+}/Fe^{3+}) varies with the preparation, from highly ordered to highly disordered. Upon cooling, the commensurate (CM) antiferromagnetic phase (AF1, $T_{N1} \approx 440$ K) with a propagation vector $\mathbf{k}_1 = (1/2, 1/2, 1/2)$ precedes an incommensurate (ICM) spiral (cycloidal) order (AF2, $\mathbf{k}_2 = (1/2, 1/2, 1/2 \pm q)$ at T_{N2} ($T_{N2} = T_S$ ranging between 150 and 310 K) [9] that persists down to the base temperature. Several works reporting fairly large electric polarization associated with the spiral phase in these perovskites [6,7] have raised great expectation due to the possibility to stabilize the spiral order even above room temperature. Investigations on single crystals are still very scarce. The absence of ferroelectricity in the YBCFO crystal of Ref. [10] ($T_S \sim 175$ K) was attributed to the lack of a cycloidal component in the horizontal spiral configuration. The orientation of the spin rotation plane is not easily predictable at present due to the influence of the preparation method. In other related compositions, such as Y(Ba,Sr)CuFeO$_5$, where T_S exceeds 300 K [11], the polycrystalline samples were too leaky to sustain electric polarization at room temperature (RT).

The exceptional stability of the spiral magnetic order in this layered structure requires a nonconventional mechanism. Though the reference compound YBCFO is not a geometrically frustrated magnet, magnetic frustration becomes present in the absence of perfect *B*-site cation order, when samples are prepared with partial Fe/Cu order in the structure (chemical disorder of the magnetic cations at the *B* site). The CM phase of YBCFO exhibits three main types of magnetic couplings [7]. In the *ab* plane, there is strong antiferromagnetic (AFM) interaction, J_{ab}, for any combination of neighboring atoms (Fe-Fe, Cu-Cu, Fe-Cu). Along the *c* axis instead, there are two different magnetic couplings. There is a weak AFM interaction Jc_1, between successive bilayers across the Y sublattice and a weak ferromagnetic (FM) coupling, Jc_2, within each bilayer across the apical oxygen (Cu-O1-Fe). The latter is the most affected by cation disorder [9]. Morin *et al.* unveiled a huge impact of cation disorder on T_S, the magnetic modulation vector and the inclination of the spiral rotation plane [9]. In an effort to justify the unexpectedly high stability of the spiral order in this double perovskite, Scaramucci and co-workers theoretically addressed the foreseeable effects of frustration due to *B*-site disorder (Cu/Fe) in this layered structure. So, the theoretical model developed by Scaramucci *et al.* describes the formation of high-T_S spiral order in nonfrustrated lattices of classical *XY* ferromagnets with only nearest-neighbor interactions when a large enough fraction of equally oriented ferromagnetic bonds are substituted by random impurity bonds presenting sufficiently strong antiferromagnetic coupling (J_{imp}) [12,13]. An antiferromagnetic impurity bond would correspond to a bipyramid composed of Fe$_2$O$_9$ instead of FeCuO$_9$ in YBCFO, and its presence induces local frustration and spin canting around it. The sense of rotation of the local spin canting can mirror Ising variables. Additionally, thanks to the identical orientation of the impurity bonds (along a single crystallographic direction, here always parallel to the *c* axis), the long-range correlations

between the local cantings are favored and can generate a magnetic-spiral order (a "ferromagnetic" Ising ground state of either clockwise or counterclockwise canting of the spins). In other words, a continuous twist can be induced parallel to the direction of the antiferromagnetic impurity bonds. The model by Scaramucci *et al.* also predicts that (i) the continuous twist ground state is favored in Bravais lattices in which neighboring impurities are closer in the plane than along the orientation of the impurity bonds. Moreover, (ii) the transition temperature (T_S) and spiral wave vector (magnetic modulation) are (for low degree of disorder) proportional to the density of antiferromagnetic impurity bonds. The proposed mechanism thus entails spiral order by disorder and could also underlay very stable noncollinear modulated orders in other very anisotropic structures (such as, e.g., some doped hexaferrites [14,15], (Fe, Cr)$_2$O$_3$ [16], etc.).

Despite the theoretical progresses achieved in the last years for modeling the spiral order by disorder mechanism, from the experimental viewpoint more precise and exhaustive investigations are still pending. This work is aimed to fill that gap, extending previous reports on the reference composition YBCFO [7,9]. In the following we report a systematic, meticulous experimental investigation of the influence of Fe/Cu cation disorder (monitored and quantified through the improper occupancy of the Fe and Cu positions) on the evolution of the noncollinear magnetic and structural properties in the YBCFO layered perovskite. The interplay between disorder, stability, and the features of the modulated spiral magnetic phase in YBCFO have been thoroughly and quantitatively described, and also analyzed in the light of the theoretical predictions. In YBCFO the influence of disorder (and only disorder) on the magnetic phase diagram, the structure, and the features of the modulated spiral is studied on a quantitative basis, extending the range of previous studies. Three different regimes are distinguished in the YBCFO phase diagram versus disorder, where a multicritical point has been found. A triple point driven by Fe/Cu disorder in YBCFO sets limits to the thermal stability of the helicoidal order and also to its cycloidal component (determined by the inclination of the spin rotation plane). Magnetic and structural mechanisms activated by disorder are analyzed in the light of the theoretical predictions. This approach paves the way to further progress for the optimization of multifunctional perovskites with high-T_S spiral magnetic order. Some conclusions also present interest for other noncollinear anisotropic or layered magnets in which the spiral order (cycloidal, conical, …) can form "by disorder" at normal working temperatures.

II. SAMPLE PREPARATION AND EXPERIMENTAL METHODS

Polycrystalline samples with identical composition YBaCuFeO$_5$ were prepared by the solid-state reaction method. High-purity Y$_2$O$_3$, BaCO$_3$, CuO, and Fe$_2$O$_3$ precursor oxides were dehydrated at 150 ℃ for 48 h. Decarbonation of Y$_2$O$_3$ oxide was achieved by a preannealing process at 900 ℃ for 10 h. Stoichiometric amounts of the oxides were then mixed, and thoroughly grounded using an automatic agate mortar for several hours until a fine and homogeneous powder was obtained. The resulting powder

was then pressed into pellets, which were heated for 50 h at 1150 °C in air. Finally, in order to obtain specimens with different degree of B-site cationic order, we applied dissimilar cooling processes to each sample. We will refer to them as Sn ($1 \leqslant n \leqslant 7$, where higher n values denote ascending Fe/Cu disorder). To samples S1, S2, and S3 we applied a controlled cooling rate of, respectively, 10 °C/h, 300 °C/h, and 450 °C/h. Samples S4, S5, S6, and S7 were obtained by quenching into liquid nitrogen or water. The quenching process consisted on pulling the sample crucible out of the tubular furnace, turning it over to drop the sample into a wide cryogenic Dewar flask containing the quenching medium. By this process samples S4 and S5 were quenched using liquid nitrogen and water, respectively. Although it is not possible to determine quantitatively the real cooling rate of quenched samples, the time elapsed between the moments in which these samples were pulled out of the furnace and got in contact with the medium was ∼ 12 s. Later on, with the aim of achieving even higher cooling rates, the process of dropping the samples into the medium was modified. By decreasing as much as possible the distance between the furnace tube and the Dewar flask, and dropping directly both crucible and sample into the medium, the process could be effectively shortened to ∼ 5 s. By this improved process samples S6 and S7 were quenched, respectively, into liquid nitrogen and water. The highest Cu/Fe disorder was obtained for the sample S7, where the quenching was done by fast cooling in liquid water.

After this, small pieces of each sample were kept solid for the macroscopic measurements, and the rest was pulverized to perform powder-diffraction experiments.

The quality of the samples was assessed by x-ray and neutron diffraction, and magnetic measurements. Laboratory x-ray diffraction patterns collected at RT using a Siemens D-5000 diffractometer ($\lambda[\text{Cu } K_\alpha] = 1.54$ Å) showed a very good crystallinity and purity of the samples within the detection limit of the technique (∼ 1%). Synchrotron radiation x-ray powder-diffraction patterns (SXPD) were collected at 300 K at the BL04-MSPD beamline [17] of the ALBA Synchrotron Light Facility (Cerdanyola del Vallès, Spain). The samples were loaded in borosilicate glass capillaries (0.7-mm diameter) and kept spinning during data acquisition. A short wavelength, $\lambda = 0.413\ 57(3)$ Å, was selected to reduce absorption and enlarge the q range. The value of λ was calibrated using a standard silicon. As the detection system, we used a high-throughput position sensitive detector MYTHEN which allows a high photon flux. The acquisition time to perform a RT full structural characterization was 90 s.

The neutron powder-diffraction (NPD) measurements were carried out at the high-flux reactor of the Institut Laue Langevin (Grenoble, France), using the high-intensity, high-resolution two-axis D20 diffractometer configured with a highly oriented pyrolytic graphite monochromator and 42º take-off angle ($\lambda = 2.41$ Å), with excellent resolution at low q and a high-efficiency position-sensitive detector covering an angular range up to 150º. Powder samples were filled into 8-mm-diameter vanadium containers. For each sample, two patterns with an acquisition time of 15 min were collected at 10 K and averaged for signal-to-noise ratio optimization. Thermodiffractograms were also collected in continuous

mode following temperature ramps within the range 10 to 500 K, with applied heating rate of 2 K/min and acquisition time of 2.5 min per scan. Around 100 patterns were recorded in the range 10 to 500 K with a resolution in temperature of 5 K between successive patterns. Finally, the end members of the series (S1, S2, and S7 samples) were also measured on D20 in the paramagnetic state (at 490 K) using a shorter wavelength ($\lambda = 1.54$ Å). The temperature range of the experiment was covered by using a dedicated helium cryofurnace.

Structural and magnetic Rietveld refinements of the x-ray synchrotron and neutron patterns were made using the Full-Prof package of programs [18]. Crystallographic tools from the Bilbao Crystallographic server [19–21] and ISOTROPY Software Suite [22] were also used. The illustrations of the crystal structure were obtained using the VESTA program [23]. The cationic disorder in each sample was determined by SXPD data analysis through the Fe/Cu occupancies at the B sites of the perovskite. It is represented by the "improper occupancy" parameter n_d (0 [full order]$< n_d \leqslant$ 0.5 [full disorder]) described in the next section. A second key parameter for the description of the samples is the modulation q_S of the incommensurate spiral magnetic phase, $\mathbf{k}_2 = (1/2,\ 1/2,\ 1/2 \pm q_S)$ being the propagation vector, directly related to n_d, which was obtained from the NPD data.

Macroscopic magnetic measurements were performed using a vibrating sample magnetometer in a Physical Properties Measurement System (Quantum Design Inc.) for recording the temperature dependence of the magnetization $M(T)$ in the interval 10–500 K under an applied external magnetic field of 2 kOe.

III. B-SITE DISORDER AND MAGNETIC INCOMMENSURABILITY

The YBaCuFeO$_5$ samples were well described using the $P4mm$ symmetry, which allows to vary the chemical disorder in the layers formed by bipyramids through a distinct occupancy of the nominal Cu and Fe sites ($1b$ sites) [7,9,11,24]. Figure S1 (Supplemental Material [SM] in Ref. [25]) displays the refined SXRD patterns for the seven YBaCuFeO$_5$ samples investigated. Table I reports the corresponding structural parameters and agreement factors at 300 K. SXRD patterns allowed to refine the atomic positions and the occupancies of the Cu and Fe ions in the two pyramids of the unit cell [Cu rich is the upper (M1) and Fe rich the lower (M2) pyramid, respectively]. For this purpose, the z coordinates of the two positions that a given metal M (either Fe or Cu) can occupy in the cell (M1 and M2) were constrained in the form $z(M1) + z(M2) = 1$. In Table I we denote as proper positions Cu1 (upper pyramid in the cell) and Fe2 (lower pyramid in the cell). In the ordered limit Cu1 and Fe2 sites are fully occupied, and hence the partial (improper) occupancy of the positions Fe1* and Cu2* is proportional to disorder. So, disorder is monitored by the improper occupancy n_d, defined as the fraction of Fe [Cu] atoms that occupy Fe1* [Cu2*] sites (see Table I). Hereinafter the improper occupancy n_d in a sample is used to parametrize its chemical disorder (related to the density of impurity bonds in Ref. [12]).

First, we have studied the influence of Fe/Cu cation disorder (n_d) on the incommensuration (q_S) of the spiral magnetic

TABLE I. Structural parameters at $T = 300$ K and agreement factors from Rietveld refinement of MSPD@ALBA synchrotron data ($\lambda = 0.413\,57$ Å).[a] The coordinates of each metal (M: Cu or Fe) are constrained by $z(M1) + z(M2) = 1$.

$T = 300$ K		S1	S2	S3	S4	S5	S6	S7
P4mm								
$a=b$ (Å)		3.874 91(2)	3.87526(2)	3.87556(2)	3.87566(2)	3.87549(1)	3.87606(1)	3.87642(2)
c (Å)		7.66432(4)	7.66278(4)	7.66236(4)	7.66056(4)	7.65962(3)	7.65974(3)	7.65917(4)
V (Å^3)		115.0792(13)	115.0771(13)	115.0885(13)	115.0675(13)	115.0433(10)	115.0789(10)	115.0915(13)
Y	z/c	0.4948(8)	0.4941(8)	0.4932(6)	0.4937(8)	0.4942(8)	0.4929(5)	0.4938(8)
$1a$ $(00z)$								
	$U_{\rm iso}$ (Å^2)	0.00245(10)	0.00204(10)	0.00354(8)	0.00177(9)	0.00379(9)	0.00350(7)	0.00328(9)
Ba	z/c	0	0	0	0	0	0	0
$1a$ $(00z)$								
	U_{11} (Å^2)	0.00689(6)	0.00666(6)	0.00750(5)	0.00666(6)	0.00768(5)	0.00765(4)	0.00764(5)
	U_{33} (Å^2)	0.0253(2)	0.0244(2)	0.02767(20)	0.0244(2)	0.0284(2)	0.02823(16)	0.0282(2)
Cu1	z/c	0.71898(37)	0.71894(52)	0.72008(45)	0.71837(49)	0.72104(63)	0.72072(45)	0.72110(68)
$1b$ $(1/2\,1/2\,z)$								
Fe1*	z/c	0.74390(50)	0.74455(93)	0.74475(81)	0.74578(94)	0.74295(93)	0.74452(78)	0.74323(96)
$1b$ $(1/2\,1/2\,z)$								
Fe2	z/c	0.25610(50)	0.25545(93)	0.25525(81)	0.25422(94)	0.25705(93)	0.25548(78)	0.25677(96)
$1b$ $(1/2\,1/2\,z)$								
Cu2*	z/c	0.28102(37)	0.28106(52)	0.27992(45)	0.28163(49)	0.27896(63)	0.27928(45)	0.27890(68)
$1b$ $(1/2\,1/2\,z)$								
	$U_{\rm iso}$ (Å^2)	0.00483(12)	0.00461(12)	0.00642(10)	0.00375(12)	0.00699(11)	0.00682(8)	0.00678(11)
O1	z/c	0.0119(13)	0.0085(17)	0.0035(14)	0.0045(22)	0.0013(28)	0.0002(20)	0.0004(29)
$1b$ $(1/2\,1/2\,z)$								
	U_{11} (Å^2)	0.00537(15)	0.00539(15)	0.00561(11)	0.00533(14)	0.00604(13)	0.00609(10)	0.00595(13)
	U_{33} (Å^2)	0.0118(6)	0.0119(6)	0.0128(4)	0.0117(6)	0.0144(5)	0.0146(4)	0.0141(5)
O2	z/c	0.3138(14)	0.3128(16)	0.3131(14)	0.3119(17)	0.3135(18)	0.3133(12)	0.3131(18)
$2c$ $(1/2\,0\,z)$								
	U_{11} (Å^2)	0.00756(15)	0.00758(15)	0.00780(11)	0.00753(14)	0.00823(13)	0.00828(10)	0.00814(13)
	U_{22} (Å^2)	0.00440(15)	0.00442(15)	0.00465(11)	0.00437(14)	0.00508(13)	0.00512(10)	0.00498(13)
	U_{33} (Å^2)	0.0055(6)	0.0055(6)	0.0064(4)	0.0053(6)	0.0081(5)	0.0083(4)	0.0077(5)
O3	z/c	0.6809(15)	0.6812(17)	0.6824(14)	0.6815(18)	0.6820(18)	0.6849(11)	0.6833(17)
$2c$ $(1/2\,0\,z)$								
	U_{11} (Å^2)	0.00756(15)	0.00758(15)	0.00780(11)	0.00753(14)	0.00823(13)	0.00828(10)	0.00814(13)
	U_{22} (Å^2)	0.00440(15)	0.00442(15)	0.00465(11)	0.00437(14)	0.00508(13)	0.00512(10)	0.00498(13)
	U_{33} (Å^2)	0.0055(6)	0.0055(6)	0.0064(4)	0.0053(6)	0.0081(5)	0.0083(4)	0.0077(5)
Occ (Cu1/Fe2)		0.706 (29)	0.684(28)	0.628(29)	0.613(28)	0.563(43)	0.594(26)	0.560(43)
Occ (Fe1*/Cu2*) $= n_d$		0.294(29)	0.316(28)	0.372(29)	0.387(28)	0.437(43)	0.406(26)	0.440(43)
χ^2		91.6	97.8	46.0	57.8	40.8	92.2	71.4
R_B		4.26	4.54	3.56	3.68	4.26	4.53	3.94
R_f		2.56	2.57	2.11	1.80	2.54	2.00	2.44

[a] Fe1* and Cu2* sites correspond to the minority fraction. n_d = disorder.

phase (full details of the magnetic orders are given in Sec. V). The values of both parameters in all the YBCFO samples investigated are listed in Table II. Figure 1 discloses the experimental relationship found between the values of the magnetic incommensurability (determined by neutron diffraction at 10 K) and the chemical disorder n_d in our YBCFO samples prepared with increasing disorder. The evolution shown in the figure proves a direct relationship between cation disorder (n_d) and the magnetic incommensurability q_S. The q_S (n_d) dependence found in our set of samples with growing disorder is satisfactorily parametrized by fitting the experimental points to a linear function (also exposed in Fig. 1):

$$q_S = -0.025(31) + 0.445(78)n_d . \tag{1}$$

The dashed lines in Fig. 1 illustrate the fitted evolution versus the *improper* occupancy n_d (occupation of Fe1* and Cu2* sites in Table I, $0 < n_d < 0.5$) and also versus the symmetrically equivalent *proper* occupation ([$1 - n_d$]: occupation of Cu1 and Fe2 sites in Table I). An improper occupation $n_d = 0.5$ would thus correspond to a random B-site cation distribution. On the other hand, the canting angle φ determined for each sample is also shown in the right axis of Fig. 1. The frequency shift q_S measures how much the spiral wave deviates from the antitranslational symmetry along **c** ($\Phi = \pi + \varphi = \pi + 2\pi q_S$). The angle Φ (see Fig. 1) stands for the rotation angle between the spins of equivalent pyramids in successive cells [7,10,26]. Therefore, Fig. 1 portrays a direct relationship between Cu/Fe disorder and the

TABLE II. Refined magnetic parameters for the spiral (10 K) and collinear (390 K) orders in YBaCuFeO$_5$ as a function of the Fe/Cu chemical disorder at the B sites of the perovskite. See explanation in the text (theta angle of the ICM phase (θ_S) in model 2 was fixed to its refined value in model 1).

	S1	S2	S3	S4	S5	S6	S7
q_S (r.l.u.)	0.09522(29)	0.11901(29)	0.12890(29)	0.15366(29)	0.16018(29)	0.17432(29)	0.17813(29)
n_d	0.294(29)	0.316(28)	0.372(29)	0.387(28)	0.437(43)	0.406(26)	0.440(43)
$r = m_L/m_S$	0.569(48)	0.606(48)	0.708(56)	0.738(56)	0.845(98)	0.777(55)	0.852(98)
T_{N1}(K)	469(8)	445(9)	432(9)	420(12)	426(12)	410(16)	422(16)
T_{N2}(K) $= T_S$	186(8)	249(9)	276(9)	345(12)	350(12)	360(16)	366(16)
Spiral order 10 K (AF2-ICM)							
Model 1 ($M_i \sim 0$)							
m_S (μ_B)	3.480(32)	3.287(35)	2.760(32)	3.175(28)	2.693(27)	2.002(38)	2.409(31)
$m_L = rm_S$ (μ_B)	1.985(18)	2.002(21)	1.954(24)	2.343(20)	2.260(23)	1.563(30)	2.049(26)
θ_S (°)	47.3(5.3)	41.9(5.1)	35.5(5.2)	36.1(3.7)	30.3(4.3)	32.7(6.0)	28.7(5.8)
Model 2 ($M_r = M_i$)							
m_S (μ_B)	2.549(23)	2.418(25)	2.042(23)	2.325(21)	1.973(20)	1.450(28)	1.755(23)
$m_L = rm_S$ (μ_B)	1.455(13)	1.473(15)	1.446(17)	1.715(15)	1.656(16)	1.132(22)	1.493(19)
θ_S (°)	47.3	41.9	35.5	36.1	30.3	32.7	28.7
χ^2	31.18	40.76	54.67	31.61	34.30	60.05	52.04
R_B	2.03	4.05	4.97	2.67	2.84	2.23	2.63
R_f	1.11	2.14	2.41	1.58	1.43	1.52	1.52
R_m	6.62	8.58	9.85	9.54	8.30	10.8	8.50
Collinear order 390 K (AF1-CM)							
m_S (μ_B)	3.34(23)	3.08(24)	2.80(21)	2.39(20)	2.10(21)	1.66(27)	1.60(27)
$m_L = rm_S$ (μ_B)	1.91(13)	1.88(15)	1.98(16)	1.77(14)	1.76(18)	1.29(21)	1.36(23)
θ_C (°)	52.7(7.6)	52.4(7.5)	52.0(7.4)	49.7(5.9)	50.6(6.9)	51.8(8.6)	49.6(7.9)
χ^2	30.82	37.67	46.98	30.84	32.79	58.41	48.77
R_B	2.04	2.78	3.66	3.19	1.84	2.45	2.68
R_f	1.20	1.75	1.90	1.74	1.14	1.63	1.66
R_m	8.46	11.2	11.4	16.5	14.6	17.7	18.0

range of the constant twist (mean canting angle $\varphi = 2\pi q_S$) between the two spins in a bipyramid M_2O_9. Notice that, taking errors into account, Eq. [1] is compatible with the lack of incommensuration in the absence of chemical disorder, although this point will be analyzed in more detail further on. As mentioned before, the key factor for the spiral phase is the fraction of c-aligned straight Fe–O–Fe superexchange bonds. The model of Scaramucci and co-workers [12,13] predicts a lineal relationship between q_S and the fraction of bipyramids with Fe–O–Fe bonds (improper Fe-Fe bonds).

In our set of YBCFO samples the Cu/Fe disorder varies in the range $0.29 \leqslant n_d \leqslant 0.44$ [27]. The maximum achieved cation disorder was $n_d = 0.44(4)$ (S7 sample), very close considering errors to the extreme limit of total cation disorder at the B-site ($n_{random} = 0.5$). Later we discuss the impact of this large Cu/Fe disorder in more detail. Figure 1 thus confirms that an excellent equivalent choice to n_d in order to quantitatively monitor the B-site chemical disorder is to consider the experimental incommensurate modulation q_S, the shift of the magnetic wave with respect to the chemical cell. Consequently, in this work we have extensively used the magnetic modulation value q_S as an alternative and very accurate quantification (determined by neutron diffraction) of the level of B-site chemical disorder in the samples.

IV. STRUCTURAL EVOLUTION DUE TO B-SITE DISORDER

The evolution of the cell parameters and volume included in Table I have been plotted in Fig. S2 (SM, Ref. [25]). The expansion in the a parameter concurs with a systematic contraction of c when disorder increases, whereas the unit-cell volume hardly changes. A certain evolution of the unit-cell dimensions changing the cooling rate applied when preparing YBCFO was earlier observed in Ref. [9]. Figures S2(a) and S2(b) disclose a linear correspondence between the cell parameters (a and c) and the incommensurability of the spiral phase (q_S). The influence of cation disorder on the tetragonal distortion ($\Delta_T \equiv c/2a$) of YBCFO is shown in Fig. 2(a), and also reveals a linear evolution with the modulation q_S of the spiral phase. The linear fit to the experimental (Δ_T, q_S) points in Fig. 2(a) yields

$$c/2a = -0.011\,53(56)q_S + 0.990\,056(86). \qquad (2)$$

To fully understand the influence of Cu/Fe disorder, beyond the creation of frustrating bonds, it is necessary to identify the key structural changes associated with disorder. Firstly, although the parameter a rises systematically as disorder increases, this lattice parameter mainly affects the perpendicular coupling terms gathered in J_{ab}. Remember that
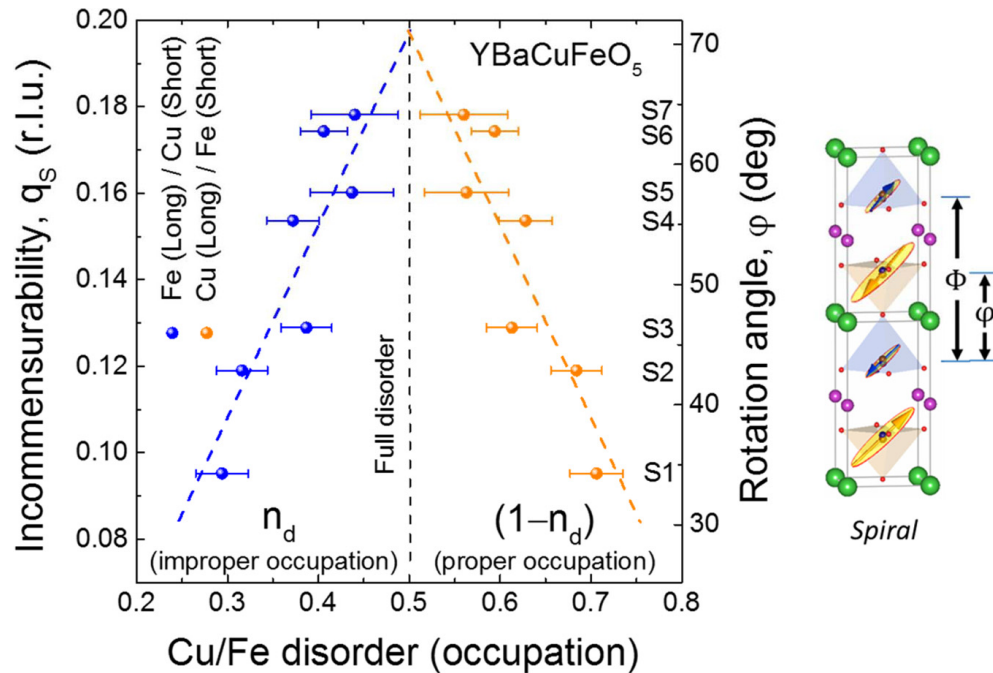
FIG. 1. Magnetic incommensurability vs *B*-site disorder. Incommensurate modulation q_S of the magnetic spiral in YBCFO as a function of its fractional Cu/Fe cationic disorder in the structure (described by the refined improper occupation n_d of Cu1 [Fe2] sites in the bipyramids). Blue (brown) points represent the improper (proper) occupation of a given pyramid. Random disorder would correspond to $n_d = 0.5$. Twist (canting) angle $\varphi = 2\pi q_S$ between the two spins in a bipyramid is shown in the right axis, and φ is also illustrated in the sketch of the spiral order that is shown on the right side. In the structural projection the blue color stands for Cu and the brown for Fe, majority in the upper ($M1$) and lower ($M2$) pyramids, respectively.

changes in this AFM term are much less relevant for T_s than changes in Jc_2 [Fig. 2(b)] induced by the compression of the lattice along the c axis. The influence of disorder on the average d_t, d_s distances and the d_t/d_s ratio is displayed in Figs. 2(c) and 2(d). d_t stands for the thickness of the bilayers and d_s for their separation [Fig. 2(b)]. It should be stressed that c contraction is caused by a systematic contraction in the thickness of the bipyramidal layers (d_t), as shown in Fig. 2(c). Such contraction is not compensated by the lesser increase of the separation between bilayers (d_s) when disorder increases. These observations agree with similar previous results reported in Ref. [11].

As Scaramucci *et al.* pointed out [12,13], magnetic frustration is activated by the presence of AFM Fe–O–Fe c bonds ($Jc_{2'}$) inside a number of bipyramids [substituting the pristine FM Fe–O–Cu bonds, (Jc_2)] [see Fig. 2(b)], whereas the Jc_1 exchange between two neighbor (successive) bilayers [separated by the distance d_S along c, Fig. 2(b)] is always AFM, independently of the Fe/Cu distribution. Additionally, we must bear in mind that bipyramids form layers where nearest-neighbors (NN) couplings in the ab plane are also always AFM, regardless of the Fe/Cu disorder. On one hand, disorder governs the density of Fe–O–Fe c bonds. On the other hand, Fig. 2(c) discloses additional concurrent lattice effects (decrease [increase] of d_t [d_s]) that are inherent to increasing Fe/Cu randomness and (in the presence of improper Fe–Fe bonds) also contribute to frustration through the tuning of the magnetic exchange couplings.

The evolution increasing disorder of z_{O1} (apical) and z_{O2} and z_{O3} (basal) coordinates is shown in Fig. 3, plotted as a function of q_S. Hereinafter we will use the term "long" pyramid (L) for that mostly occupied by Cu, and "short" pyramid (S) for that mostly occupied by Fe [see Fig. 4(a)]. The thickness of the bipyramidal layer is given by $d_t = H_L + H_S$, the sum of the heights of the two pyramids sharing the O1 (apical) atom [see Figs. 2(b) and 4(a)]. In addition to O1 the heights depend on the z position of the basal oxygens: O2 and O3 in, respectively, the S- and L-pyramids. From a quick glance at the atomic shifts shown in Fig. 3 (plotted using the same scale range), it is apparent that the shift of the apical oxygen is the primary responsible for the changes in the heights H_L, H_S and the layer thickness d_t. In Fig. 3(d) we have illustrated the relative atomic shifts in the YBCFO samples investigated with increasing the structural disorder. The shifts along-z are shown for all the atoms taking the Ba position as fixed reference. Moreover, Fig. S3 (SM, Ref. [25]) displays all the interatomic M-M distances. The Cu1-Fe1* (or Fe2-Cu2*) distance deduced from their refined positions within the same pyramid does not change –within error– increasing the disorder.

A. Impact of the Fe/Cu disorder on the evolution of the pyramids

So, it has been found that by far the largest atomic displacement generated by increasing *B*-cation disorder corresponds to shifting apical O1 atoms parallel to **c**. The main conse-
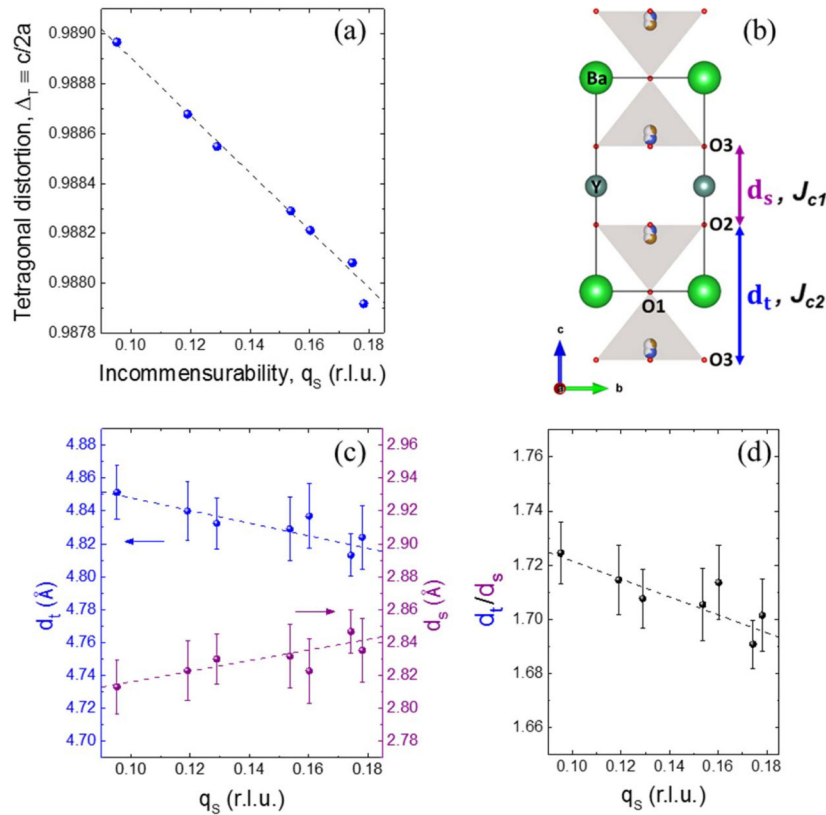
FIG. 2. Influence of disorder on the thickness and separation of the bilayers. (a) Linear dependence of the tetragonal distortion ($\Delta_T \equiv c/2a$) on the incommensurability q_S of the spiral phase (in relative lattice units, r.l.u.). (b) Projection of the $P4mm$ structure showing the thickness d_t of a bilayer and the separation d_s between bilayers. (c) Evolution of the thickness of the bipyramidal layer (d_t, left axis) and of the separation between bilayers (d_s, right axis). (d) Ratio d_t/d_s when increasing B-site chemical disorder in YBCFO. Dotted lines are linear fits to data points which are reported in Table III.

quence of such displacement is the shrinkage of the long pyramid (Cu) and the concomitant stretching of the short pyramid (Fe). For more clarity, Fig. 4(b) displays the obtained evolution of the heights of both pyramids (H_L and H_S) as a function of the Cu/Fe disorder. Their heights in angstrom are plotted versus the incommensurability of the spiral order (q_S) in each sample. Notice that disorder tends to make them more uniform, and so, due to the extreme level of disorder achieved, we obtained samples with average pyramids having practically identical sizes. In order to precisely understand the evolution shown in Fig. 4(b), it is important to pay attention to the evolution of the individual metal-to-oxygen distances in the pyramids of the compound when B-site disorder increases. Such dependence is shown in Figs. 4(c) and 4(d) as a function of q_S. Moreover, the main interatomic distances in the structure are gathered in Table S1 (SM, Ref. [25]). The distances displayed in Figs. 4(c) and 4(d) are the M–O bond lengths for the majority metal in each pyramid. A look at Fig. 4(c) confirms severe changes in the average Jahn-Teller splitting between basal and apical distances around Cu^{2+} ($t_{2g}^6 e_g^3$). The large difference between Cu-O1 (apical) and Cu-O3 (basal) coordination distances in the Cu-rich pyramid (long one) decreases from 15.4% down to the 9.7% in the most disordered sample. In other words, whereas the basal Cu-O3 is hardly modified, the apical Cu–O1

bond shrinks 5% (-0.11 Å). Figure 4(c) thus proves that the reduction in the average Jahn-Teller splitting around Cu is significant but nevertheless only partial. Notice that in Fig. 4(c) distances are taken with respect to the Cu position, whereas they are taken with respect to the Fe position in Fig. 4(d). In the short pyramid (Fe rich) described in Fig. 4(d) the average apical Fe-O1 distance remains always shorter than the basal one (Fe-O2), but increases with disorder from -6% up to $\sim -1\%$ ($+0.10$ Å). In the most disordered sample (S7), apical and basal Fe–O bonds in the short pyramid are closely similar, and the heights H_L and H_S fully comparable ($H_L \approx H_S$).

V. MAGNETIC PHASE DIAGRAM VERSUS Fe/Cu CHEMICAL DISORDER IN YBaCuFeO₅

A. Magnetic transitions

The magnetic transition temperatures were identified by susceptibility and neutron-diffraction measurements. The magnetic susceptibility curves $\chi(T)$ are shown in Fig. 5, from 5 to 500 K, as obtained in field-cooling (FC) conditions using a DC magnetic field of 2 kOe. Two local maxima in $\chi(T)$ identify the two separated transitions. The commensurate (T_{N1}) and incommensurate ($T_{N2} = T_S$) magnetic orders were comparatively investigated by neutron diffraction within the
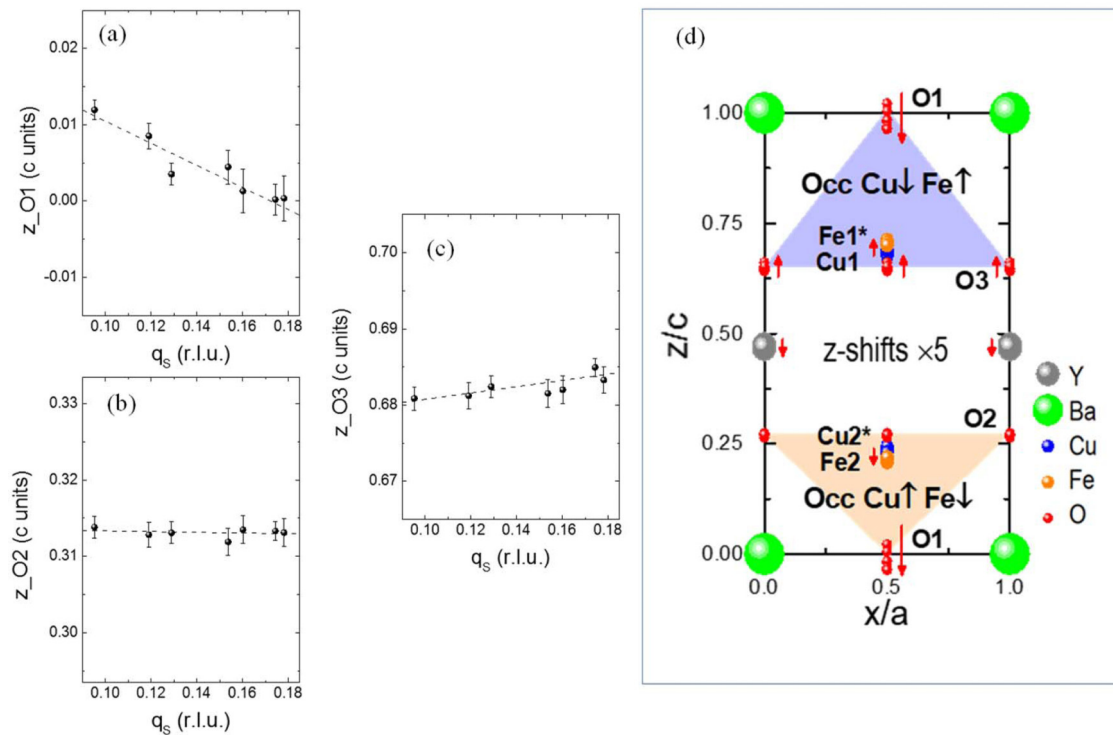
FIG. 3. Atomic shifts of apical and basal oxygens vs B-site disorder. (a), (b), (c) Evolution of the z coordinate for O1 (apical), O2, and O3 (basal) oxygens increasing Cu/Fe disorder, plotted against q_S (incommensurability). Height of the L- and S pyramids is given by $H_L = c(1 + z_{O1} - z_{O3})$; $H_S = c (z_{O2} - z_{O1})$. (d) Schematic projection of the YBCFO structure illustrating the magnitude and direction of the atomic shifts along the z axis in samples with increasing B-site disorder.

10–500 K range to elucidate the influence of increasing the level of Fe/Cu disorder in YBCFO.

Figure 6(a) shows the $T - Q$ projections of the NPD intensities collected between 10 and 500 K. The figure focuses on a Q range around the (1/2 1/2 1/2) peak that covers the main magnetic reflections. The onset and evolution of the two magnetic phases is shown. Upon cooling from 500 K, first peaks indexed as ($h/2$, $k/2$, $l/2$) appear at T_{N1} ($T_{N1} > 400$ K in all the samples). The propagation vector $\mathbf{k}_1 = (1/2, 1/2, 1/2)$ of the collinear phase sites at the A point of the Brillouin zone. T_S is easily identified in all the samples by the apparition of a set of magnetic Bragg reflections (satellites) with propagation vector $\mathbf{k}_2 = (1/2, 1/2, 1/2 \pm q)$. Throughout the paper this phase is referred to as "spiral phase," although further on we will point out certain limitations of the neutron-diffraction data obtained from powder samples. In all the samples a spiral order emerges at T_{N2} (T_S) and persists down to the base temperature [Figs. 6(a) and 6(b)].

The temperature evolution of the spiral modulation $q_S(T)$ was obtained for all the samples and it is exposed in Fig. 6(c), where the influence of disorder is immediately appreciable. The smooth decreasing evolution of $q_S(T)$ approaching T_S in the more ordered samples (low n_d) strongly contrasts with a very rapid downfall at the collinear-to-spiral transition in the most disordered YBCFO specimens. The observed change is consistent with an evolution of the transition from second to first order when the triple point approaches. At the triple point this collinear-spiral transition meets the second-order

paramagnetic-collinear ordering. In the A-site substituted $YBa_{1-x}Sr_xCuFeO_5$ family quenched in liquid nitrogen [11] a similar abrupt $q_S(T)$ evolution approaching T_S was reported in the sample with Sr content $x = 0.40$, with higher T_S and $q_S = 0.175$. The model of Scaramucci *et al.*, based on orientationally correlated Fe–O–Fe bonds, is compatible with a critical value $n_{crit} \lesssim 0.50$, above which the transition becomes of first order [13]. Our neutron results and the $q_S(T)$ evolutions depicted in Fig. 6(c) suggest a first-order collinear-to-spiral transition in YBCFO samples approaching the triple point (for a chemical disorder $n_d > \approx 0.44$ ($q_S > \approx 0.17$ r.l.u.). In contrast, the evolution exposed in Fig. 6(c) for more ordered samples rather suggests a continuous (second-order) transition. Discerning whether n_{crit} is indeed reached before the triple point or coincides with the merging of the two transitions into a single direct transition (paramagnetic-spiral) is out of the scope of this work. It would require a specific study using additional techniques and more compositions near the triple point (with controlled homogeneous disorder).

Figure 7(a) discloses a complete n_d-T magnetic phase diagram for the YBCFO system. In the horizontal axis we have represented the B-site disorder n_d obtained by Rietveld refinement in our samples. As in the preceding sections, aside from the disorder n_d and given that the chemical composition is not varied, the incommensuration q_S of the spiral is also used to typify the increasing cationic disorder in B sites (upper horizontal axis). It is worth noting that in practice the experimental accuracy for assessing q_S is greater than the
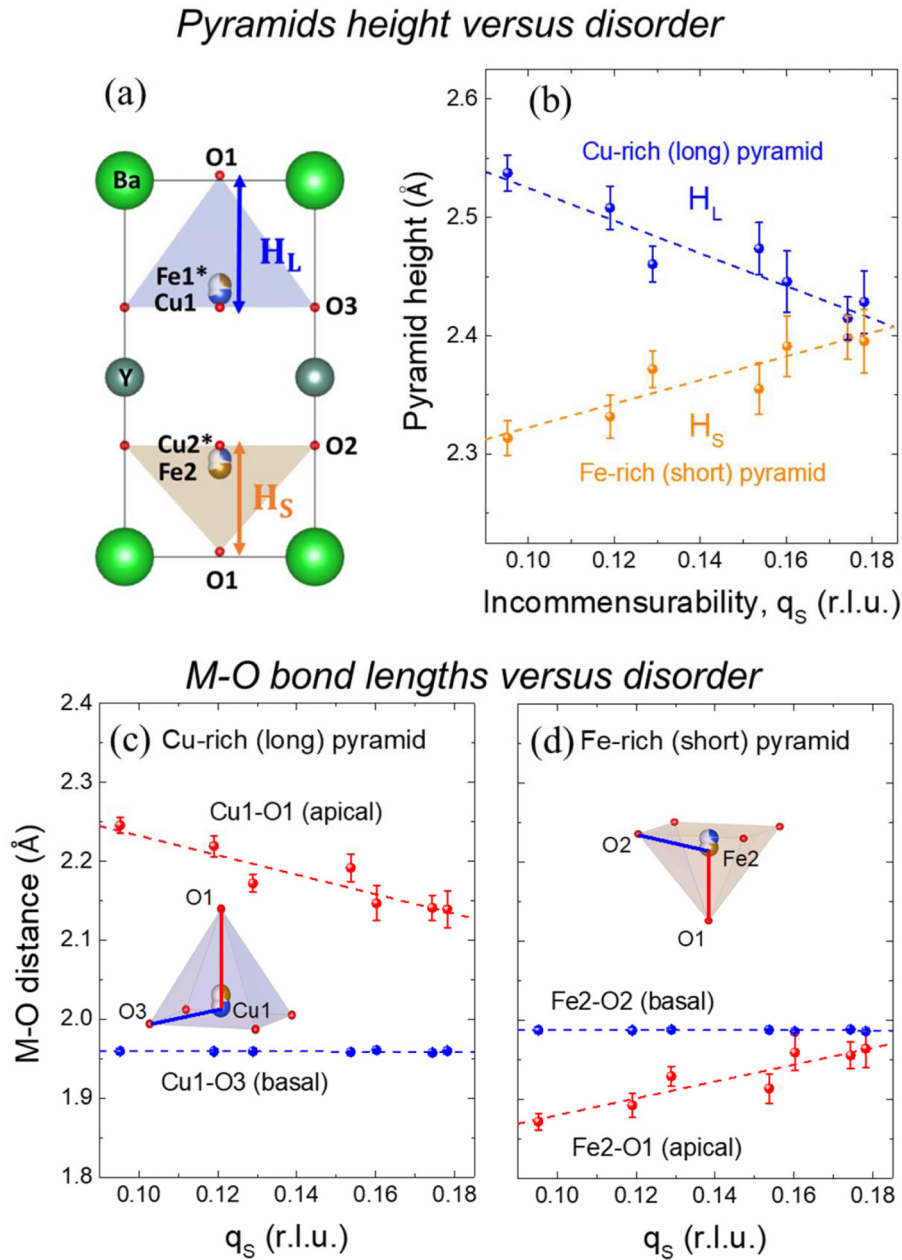
FIG. 4. Evolution of the two pyramids vs *B*-site disorder: H_L, H_S, and the average CuO$_5$ Jahn-Teller splitting. (a) Scheme of the structure illustrating the long (upper, Cu-rich) and short (lower, Fe-rich) average pyramids of the chemical unit cell. (b) Experimental correlation between the height of the two pyramids (at 300 K) and the incommensurability q_S of the spiral magnetic order when increasing Fe/Cu chemical disorder in YBCFO. CuO$_5$ pyramids are longer than FeO$_5$ ones in virtue of the Jahn-Teller distortion. Evolution increasing the disorder of the (c) Cu-O and (d) Fe-O interatomic distances in the two pyramids. Evolution of the apical and basal (equatorial) distances in both pyramids (illustrated in the insets) is shown.

accessible accuracy for the occupation n_d. For the sake of comparison, in Fig. 7(b) we show together the experimental (q_S, T_S) points of this work (in red color) and those from the YBCFO samples (in black color) reported earlier in Ref. [11]. The overall picture is thus consistent with previous studies reporting a positive variation of T_S and a negative slope of T_{N1} when the cooling rate of the prepared YBCFO samples is increased [9,11]. In the light of the phase diagram shown in Fig. 7(a), it is important to underline several noteworthy issues:

(i) As expected, the Néel temperature associated with the collinear commensurate order decreases in YBCFO when magnetic frustration increases, but the downward slope is quite smooth compared to the upward slope for T_S. The dashed lines in Fig. 7(a) are linear fits to T_{N1} and T_S, respectively. They are detailed in Table III.

(ii) Our fit of the experimental (q_S, T_s) points confirms the linear relationship predicted in the theory, in which the incommensurate wave vector and the spiral temperature are both proportional to the concentration of improper Fe-Fe
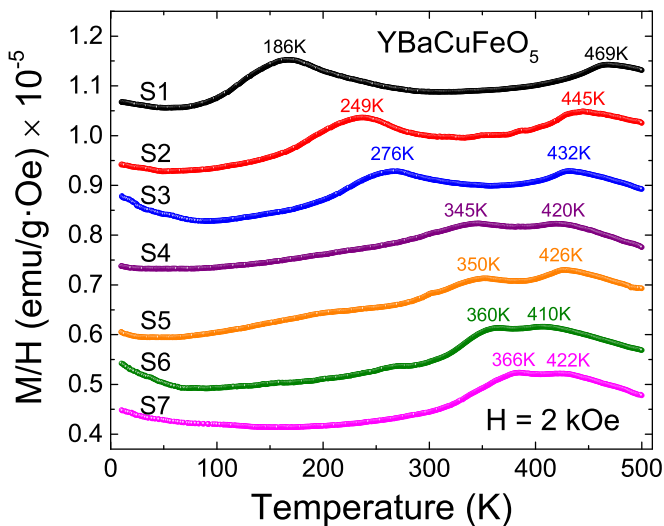
FIG. 5. Evolution of the magnetic susceptibility curves (measured in FC, 2 kOe) for YBCFO samples with increasing Fe/Cu cationic disorder. Successive curves were shifted by $+10^{-6}$ emu g^{-1} Oe^{-1} for clarity. Higher transition signals the onset of the collinear order (T_{N1}, $\mathbf{k}_1$); lower corresponds to the non-collinear spiral transition ($T_{N2} = T_S$, $\mathbf{k}_2$).

bonds [11]. However, an interesting feature is the intersection point with the *x* axis. It is noteworthy from Fig. 7(a) that the linear extrapolation does not go through the origin ($q_S = 0$, $T_s = 0$), in contrast with the usual assumption in previous reports. Remarkably, the horizontal axis ($T_s = 0$) is cut at a point q_0 (and at n_0), both related by Eq. (1) clearly separated from the origin: $q_0 = 0.025$ r.l.u. and $n_0 \approx 0.112$. It is worth mentioning here that the additional point at [$n_d = 0.10(3)$, $T_s = 0$] shown in Fig. 7(a) is taken from Ref. [28], which reports a highly ordered YBCFO single crystal (with 5% Mn doping) presenting $k1$ and $k3$ phase coexistence and lack of spiral order. Consequently in this structure there is a critical threshold of disorder (n_0) or minimum frustration level, below which a long-range spiral magnetic state cannot be formed. Such critical disorder tells us that if the concentration of straight Fe–O–Fe bonds is too low and they are too far apart, the dipolar interaction (mediated by spin waves) between individual canted spins in the vicinity of the separated Fe-Fe bonds decay without forming a coherent spiral. From the obtained q_0 critical value an estimation of the associated minimum canting angle yields $\varphi_0 \approx 9°$ ($\varphi_0 = 2\pi q_0$).

(iii) The critical threshold n_0 to achieve a spiral ground state entails the existence of an inhomogeneous region in the phase diagram when disorder is too low [$0 < n_d < n_0$ in Fig. 7(a)]. In this antiferromagnetic perovskite the ferromagnetic Jc_2 exchange between Fe^{3+}/Cu^{2+} ions within "ordered" FeCuO$_9$ bipyramids leads to the antitranslation $k_z = 1/2$. The perfectly ordered YBCFO system ($n_d = 0$) is thus expected to be of $\mathbf{k}_1$ type. Conversely, when the order is not totally perfect but it approaches, then there is a minority fraction of nonmixed M_2O_9 bipyramids ($M =$Fe or $M =$Cu), in which the M-O-M exchange is antiferromagnetic. If that fraction is still too small to form spiral ordering, phase segregation can occur, favored by the presence of short-ranged minority re-

gions with tendency to $k_z = 0$ (nonmixed AM_2O_9 bipyramids with internal antiferromagnetic coupling). So, in the region with just incipient disorder, dominant $\mathbf{k}_1 = (1/2, 1/2, 1/2)$ magnetic regions with high-T_{N1} values could coexist at lower temperatures with a small fraction of short-ranged $\mathbf{k}_3 = (1/2, 1/2, 0)$ magnetic clusters (AF3 collinear phase). These could exhibit a dynamic nature before eventually freezing out when cooling down. Recently, segregated $\mathbf{k}_3$-type collinear domains (AF3) were observed in highly ordered single crystals (with absence of spiral order) dominated by $\mathbf{k}_1$-type collinear ordering [28]. Thus, an inhomogeneous regime is anticipated in the phase diagram of Fig. 7(a) when disorder is still incipient ($n_d \to 0$ and $n_d < n_0$) and the cross talking between (too far apart) AFM Fe-Fe "defects" cannot stabilize a magnetic spiral.

(iv) From the slope of the linear $T_S(q_S)$ dependence described in Table III for the YBCFO perovskite we obtain $T_S/|q_S| \approx 71(3)$ meV, in very good agreement with the estimation of 68 meV made in the model by Scaramucci *et al.* in Ref. [13].

(v) Of utmost importance is the presence of seemingly a paramagnetic-collinear-spiral triple critical point in the phase diagram of Fig. 7(a). The triple point marks a stability limit for the spiral phase, where the collinear and spiral lines intersect and fluctuation phenomena give way to another regime. It unveils that the critical incommensurability for YBCFO is given by $q_s^c \approx 0.18$ r.l.u. and the critical propagation vector $\mathbf{k}_2^c = (1/2, 1/2, 1/2 \pm q_s^c)$. The maximum incommensuration previously reported in YBCFO was $q_S = 0.14$ r.l.u. in a quenched sample ($T_S = 310$ K) [9], although a triple point in AA'CuFeO$_5$ was first proposed by Shang *et al.* in YBa$_{1-x}$Sr$_x$Cu Fe O$_5$ samples quenched into liquid nitrogen. The stability range of the spiral was further extended by the application of chemical pressure instead of Fe/Cu disorder, reaching $T_S \approx 375$ K and $q_S \approx 0.175$ r.l.u. in the YBa$_{0.6}$Sr$_{0.4}$CuFeO$_5$ solid solution [11]. Given that divalent A cations are located within the bilayer spacing, smaller Sr^{2+} ions (with respect to Ba^{2+}) produce a compression of the bilayers in YBa$_{1-x}$Sr$_x$CuFeO$_5$, reducing d_t and increasing T_S by enhancing the AFM coupling ($Jc_{2'}$) inside the Fe$_2$O$_9$ bipyramidal units (impurity bonds). Our study of the YBCFO perovskite unveils that a triple point can be attained in this layered structure without increasing the number of divalent or trivalent chemical species in the structure. Later on we will come back to the triple point in YBCFO.

Next, we will describe how to control relevant details of the magnetic anisotropy and the magnetic spirals through the degree of *B*-site chemical order in these layered $(AA')(BB')O_5$ perovskites, keeping invariant their chemical composition in both the A and the B sites.

B. Influence of *B*-site disorder on the magnetic easy axis

We have investigated the impact of disorder on the magnetic anisotropy of YBCFO by means of neutron diffraction. Henceforth we call the orientation of the collinear magnetic moments in the commensurate phase "magnetic easy axis." As shown in Fig. 8(b), it is defined by the inclination angle θ that the moments (or the spiral plane in the incommen-
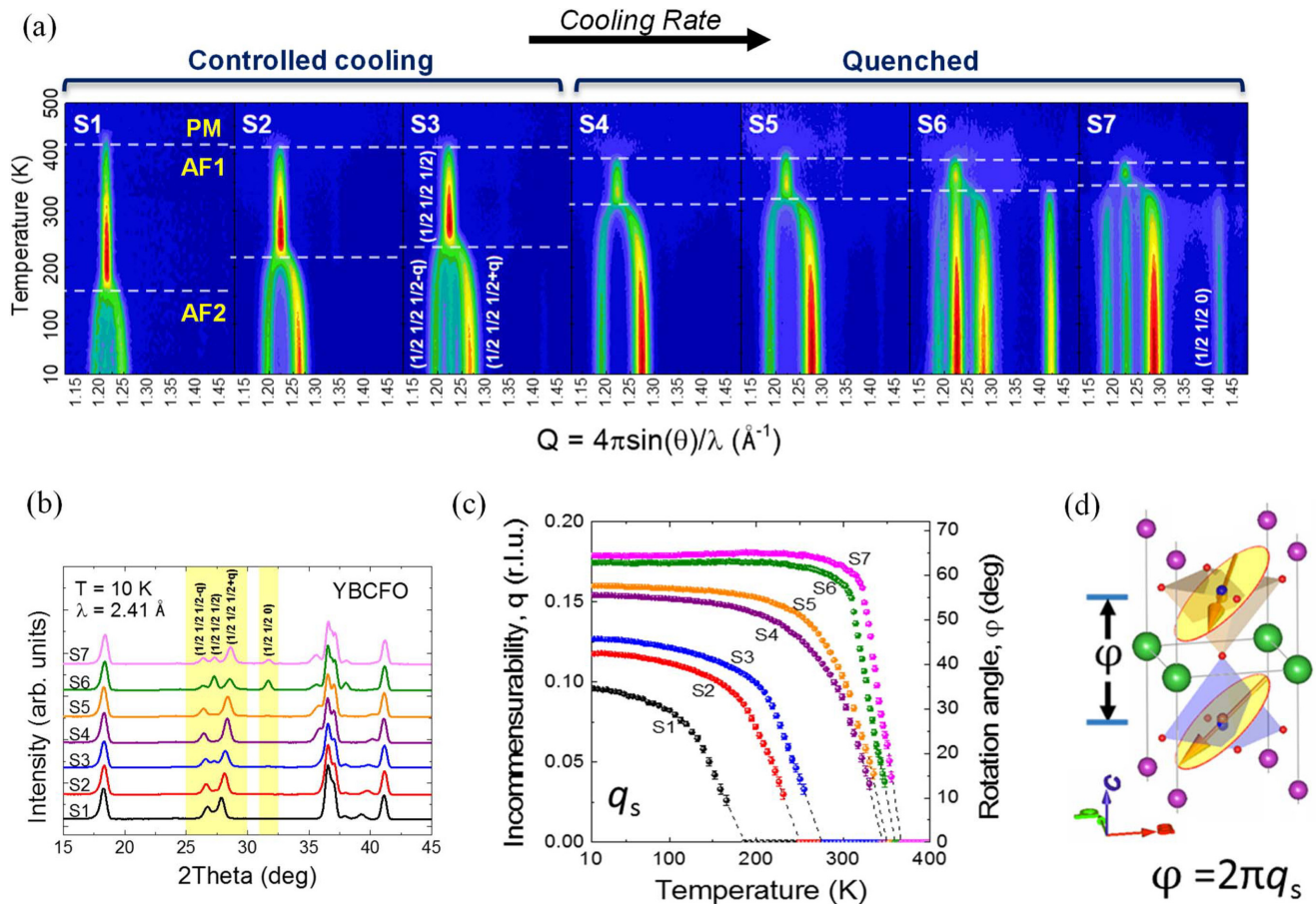
FIG. 6. Neutron diffraction in YBCFO: influence of *B*-site chemical disorder. (a) Contour maps showing the $T - Q$ projection of the temperature dependence for the neutron-diffracted intensities around (1/2 1/2 1/2) magnetic reflection (D20@ILL). Neutron intensities illustrate the emergence of the commensurate and incommensurate (spiral) magnetic phases. (b) Low-angle region of the neutron-diffraction patterns recorded at 10 K. Evolution increasing the Fe/Cu disorder.(c) Influence of chemical disorder on the incommensuration q_S of the spiral phase and its temperature dependence on YBCFO. Dashed lines are lineal extrapolations used to identify the spiral transition temperatures. (d) Illustration of the twist angle φ (canting) formed by the two spins of a bipyramid in the spiral phase ($\varphi = 2\pi q_s$).

surate case) form with the *c* axis. Notice that due to the tetragonal symmetry of the parent cell, it is not possible from NPD distinguishing the orientation of the magnetic easy axis component parallel to the *ab* plane. Any orientation of that component does not produce changes in NPD intensities. With the aim of studying the influence of chemical disorder on the magnetic easy axis, the collinear spin order in the $2a \times 2a \times 2c$ magnetic cell was refined in all the samples at 390 K. Table II reports the θ_c values obtained in the collinear regime, as well as the refined magnetic moments. Given that the theoretical ratio $m(Fe^{3+})/m(Cu^{2+})$ of their respective unpaired spins is 5, we imposed in the neutron refinement that the ratio *r* between the ordered moments at the two pyramids should be

$$r \equiv m_L/m_S = (1 + 4n_d)/(5 - 4n_d), \tag{3}$$

where n_d stands for the improper occupation factor (associated with the migrated cations) and m_L, m_S are the ordered magnetic moments refined at the long (Cu) and short (Fe) pyramids, respectively. We found that disorder has no influence on the orientation of the easy axis in the AFM collinear phase ($\mathbf{k}_1$). The spin orientation is found at $\theta_c \approx 50°$ in all the samples, no matter the level of disorder. We observed

in addition that the orientation θ_c of the magnetic easy axis was temperature independent in the collinear regime (see also Ref. [26]). To illustrate this, in Fig. 8(c) we show as an example the thermal evolution of the inclination angle $\theta(T)$ for sample S2 for the two magnetic regimes (θ_c and θ_S). The inclination of the spiral rotation plane (θ_S) is very similar (although slightly lower) and equally remains very stable below T_S. Contrasting with the collinear easy axis, in the next section we will explore and describe a very different response to disorder of the characteristic spin rotation plane of the spiral phase.

C. Influence of *B*-site disorder on the anisotropy of the spiral phase

1. Limitations of the neutron powder diffraction

In a powder-diffraction pattern all the reciprocal space is projected onto one dimension, as a function of 2θ. Therefore, all reflections located at the same 2θ angle contribute to a unique peak of the pattern, whose intensity results from all those peaks. In contrast to single-crystal diffraction measurements, where each single reflection is collected individually, the averaging inherent to NPD entails limitations that in the
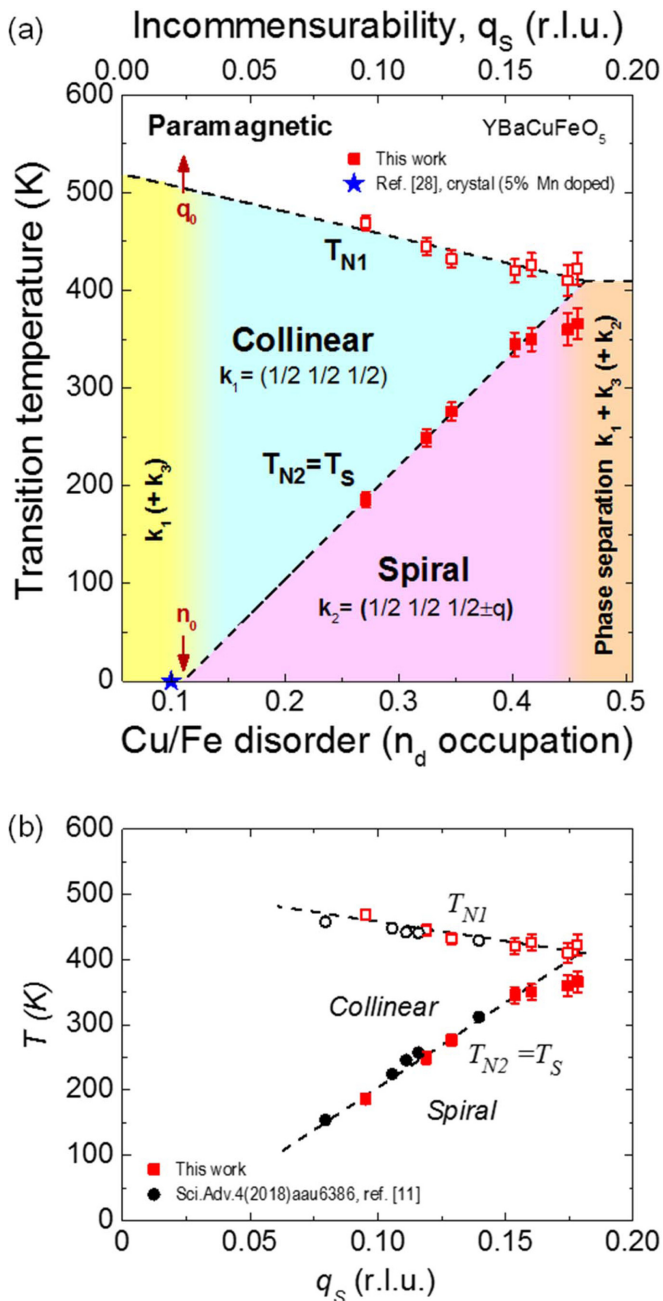
FIG. 7. Magnetic phase diagram vs Fe/Cu chemical disorder for YBaCuFeO$_5$. (a) n_d–T magnetic phase diagram for YBCFO. Phase boundaries describe the onset of the magnetic phases according to neutron-diffraction data. (b) q_S-T plot for YBCFO, including the points from samples reported in Ref. [11].

case of cycloidal or helicoidal orders may prevent its complete description. In the case of magnetic structures, in addition to projecting onto a single dimension, only the perpendicular component of the magnetic structure factor to the scattering vector contributes to the intensity of each reflection. A more detailed example about the limitations of NPD to fully characterize incommensurate spiral orders can be found in Ref. [29]. NPD data collected in our set of YBCFO samples are compatible with an incommensurate spiral phase below

T_S, described in the form

$$
\boldsymbol{m}_{lj}(\boldsymbol{k}) = M_R(\boldsymbol{m})(\boldsymbol{u}_j)\cos\left(2\pi\{\boldsymbol{k}.\boldsymbol{R}_l + \Phi_J\}\right)
$$
$$
+ M_I(\boldsymbol{m})(\boldsymbol{v}_j)\sin\left(2\pi\{\boldsymbol{k}.\boldsymbol{R}_l + \Phi_J\}\right), \qquad (4)
$$

where $\boldsymbol{m}_{Ij}$ is the magnetic moment of the atom j in the unit cell l, $\boldsymbol{R}_l$ is the vector joining the arbitrary origin to the origin of unit cell l, and Φ_j is a magnetic phase. $\boldsymbol{u}_j$ and $\boldsymbol{v}_j$ designate the orientation of the two perpendicular unitary vectors that define the plane of the helix, where M_R (real) and M_I (imaginary) amplitudes fix the dimensions of the elliptical envelope described by the rotating magnetic moments.

In these powder samples (due to the intrinsic limitations mentioned above) it is not possible to independently refine (i) the real and imaginary amplitudes (M_R and M_I) or (ii) the two magnetic moments in the bipyramidal units, forcing us to fix their ratios using constraints. Hence the neutron patterns were refined constraining the two ordered moments (at the long and short pyramids) according to the ratio $r(r \equiv m_L/m_S)$ deduced from the refined occupations (disorder) for each sample [see Eq. (3)] and listed in Table II. Moreover, the two moments of a bipyramid were restricted to the same inclination angle θ in the neutron refinements. Additionally, the phase difference between the magnetic moments at the two pyramids separated by the Y layer in the chemical cell was fixed to 180° as found in Refs. [6,7,9,10] (during the data analysis we confirmed that any deviation from 180° when comparing the different samples should be lower than 2 °–3°).

It is necessary to stress that the most relevant drawback of studying powder samples of this layered structure probably is the inability to refine the real and imaginary amplitudes (M_R and M_I) of the elliptical spiral order. In other words, identical agreement factors are obtained regardless of the chosen M_I/M_R ratio. So, we decided to extend the study of the incommensurate magnetic order to include the two opposite limits of (i) very large ($M_R \gg M_I$) and (ii) null eccentricity ($M_R = M_I$). The latter picture has been adopted in the majority of earlier works and agrees well with the tetragonal symmetry of the paramagnetic structure.

In Table II we list the refined magnetic moments (m_L, m_S), modulation vectors (q_S), and tilting angles θ_S of the rotating plane of the spins (easy plane) for the incommensurate magnetic phase obtained from NPD data at 10 K. This table exposes the information of the incommensurate magnetic phase in YBCFO samples with increasing magnetic frustration induced by raising the level of Fe/Cu disorder (quantified through n_d and q_S). The two opposite extremes or limits mentioned before were considered and are shown in the table: $M_R \gg M_I$ (model 1) and $M_R = M_I$ (model 2). The former limit draws a collinear sinusoidal order ($M_I = 0$) and the second one describes a circular spiral. Keep in mind that intermediate eccentricities ($0 < M_I/M_R < 1$) between the two extremes are also compatible with recorded NPD patterns. A study of the possible changes in the eccentricity induced by disorder would require single crystals. In order to minimize the uncertainty in the refined θ_S values, first we used the $M_R \gg M_I$ limit for obtaining this tilting angle below T_S. Then, this refined θ_S value was used in the magnetic refinement of the circular spiral (model 2). This allows to maximize accuracy, minimizing the errors in the determination of θ_S. The full

TABLE III. Regression slopes and intercepts obtained from linear least-squares regression fits to key structural and magnetic parameters in the layered YBaCuFeO$_5$ structure obtained from Rietveld refinement of x-ray and neutron powder diffraction data as function of the incommensurability q_S. The goodness of the regression model R^2 and standard error of the intercept and slope (A and B, respectively) are shown. In the case of θ_S as function of q_S, a regression model with an additional quadratic coefficient C was used.

Equation	A	B	R^2
$a = A + Bq_S$	3.87354(60)	0.0139(38)	0.8247
$c = A + Bq_S$	7.67016(83)	$-0.0621(55)$	0.9750
$V = A + Bq_S$	115.084(47)	$-0.09(31)$	0.0152
$\Delta_T \equiv c/2a = A + Bq_S$	0.990056(86)	$-0.01153(56)$	0.9908
$q_S = A + Bn_d$	$-0.025(31)$	0.445(78)	0.8435
$d_t = A + Bq_S$	4.886(13)	$-0.383(87)$	0.7481
$d_s = A + Bq_S$	2.784(13)	0.322(91)	0.6446
$d_t/d_s = A + Bq_S$	1.755(13)	$-0.331(86)$	0.6888
$H_L = A + Bq_S$	2.663(32)	$-1.38(23)$	0.8795
$H_S = A + Bq_S$	2.222(27)	1.00(19)	0.8394
$z_{O1} = A + Bq_S$	0.0250(32)	$-0.145(24)$	0.8902
$z_{O2} = A + Bq_S$	0.3138(11)	$-0.0045(77)$	0.0564
$z_{O3} = A + Bq_S$	0.6766(21)	0.041(14)	0.5769
$d(\mathrm{Cu} - \mathrm{O}_a) = A + Bq_S$	2.35581(93)	$-1.2362(67)$	0.8507
$d(\mathrm{Cu} - \mathrm{O}_b) = A + Bq_S$	1.9612(40)	$-0.016(25)$	0.0209
$d(\mathrm{Fe} - \mathrm{O}_a) = A + Bq_S$	1.773(25)	1.07(19)	0.8438
$d(\mathrm{Fe} - \mathrm{O}_b) = A + Bq_S$	1.9888(35)	$-0.011(22)$	0.1015
$T_{N1} = A + Bq_S$	517.2(15.7)	$-590.9(106.5)$	0.8602
$T_{N2} = T_S = A + Bq_S$	$-61.7(9.9)$	2610.1(78.6)	0.9961
$\theta_S = A + B \cdot n_d$	78.8(3.1)	$-112.8(8.1)$	0.9776
$\theta_S = A + Bq_S + Cq_S^2$	$A = 84.1(30.6)$; $B = -488.4(457.9)$; $C = 1044.0(1663.6)$		0.8949

neutron Rietveld refinements (at 10 K, using model 2) for all our YBCFO samples are exposed in Fig. S4 and the extracted magnetic information is listed in Table S2 (SM, Ref. [25]).

2. Influence of chemical disorder on the inclination of the magnetic spiral plane

As mentioned before, we use the angle θ to describe the angular distance (inclination) between the direction of the spins and the **c** axis, in the collinear and noncollinear phases. In the former the magnetic easy axis is given by the collinear spin direction **u** (CM phase). In the spiral ICM phase at $T < T_S$ θ_S describes the tilting of the rotation plane of the helix [uv plane; see Eq. (4) and Fig. 8(b)]. The tetragonal symmetry prevents specifying the orientation of the moments in the ab plane. For simplicity, the director vector **u** can be taken as within the ac plane, **v** being thus parallel to the b axis. θ_S values close to zero mean the magnetic easy axis is close to the **c** axis, whereas $\theta_S \approx 90°$ implies that the easy axis is parallel to the ab plane. Morin *et al.* were the first to report changes in the inclination angle in YBCFO samples prepared changing the cooling rate. Only for $\theta_S = 0°$ or $90°$ do all the active magnetic modes describing the magnetic arrangement belong to the same magnetic irreducible representation [7].

Figure 8(a) plots the experimental (q_S, θ_S) points obtained from neutrons at 10 K. The figure illustrates the systematic decrease of θ_S (within the range $\sim 50°$–$30°$) in YBCFO samples with increasing disorder [q_S or n_d; the (n_d, θ_S) plot is also shown]. The observed $\theta_S(q_S)$ evolution is satisfactorily described by a parabolic fit. We should call to mind that the orientation of the plane of the helix with respect to the

c axis (axis of the magnetic modulation, with k_z orientation) determines if the spiral order resembles more a cycloid ($\theta_S \to 0°$) or a helix ($\theta_S \to 90°$). The observed reorientation of the spiral plane agrees with earlier works reporting a greater misalignment with respect to the tetragonal plane in samples prepared by fast cooling (more disordered) [9,11]. Keep in mind that in the presence of spin-orbit coupling and effective DM terms (or spin-current mechanism triggering magneto-electric coupling), the expected dependence of the electrical polarization magnitude P with the orientation of the helix is of the type $P \alpha Q \cos(\theta_S)$ (Q: spin chirality, different from zero in the noncollinear phase). Hence, in this scenario, a cycloidal order ($\mathbf{Q} \perp \mathbf{c}$) might be more favorable to ferroelectricity than a pure helix ($\mathbf{Q} // \mathbf{c}$).

Additionally, we wanted to examine the dependence of the tilting (θ_S) on –directly– the Fe/Cu disorder monitored by the occupation n_d. This is plotted as an inset in Fig. 8(a). This plot unveils a noteworthy finding. Interestingly, we reveal a linear relationship between the spiral's tilting angle and the level of Fe/Cu cation disorder in these layered perovskites, parametrized by the improper occupation n_d. The linear fit to the experimental (n_d, θ_S) points is shown in the inset of Fig. 8(a). It shows that the linear relationship is very well suited and the linear parameters found are given in Table III [30].

Figure 9(a) displays the projection of the incommensurate magnetic structures described in Table II, refined at 10 K using the circular spiral model ($M_R = M_I$). Two complementary projections are plotted for each sample, which help to illustrate the inclination of the spiral plane in each of the seven YBCFO specimens with gradually larger disorder n_d.
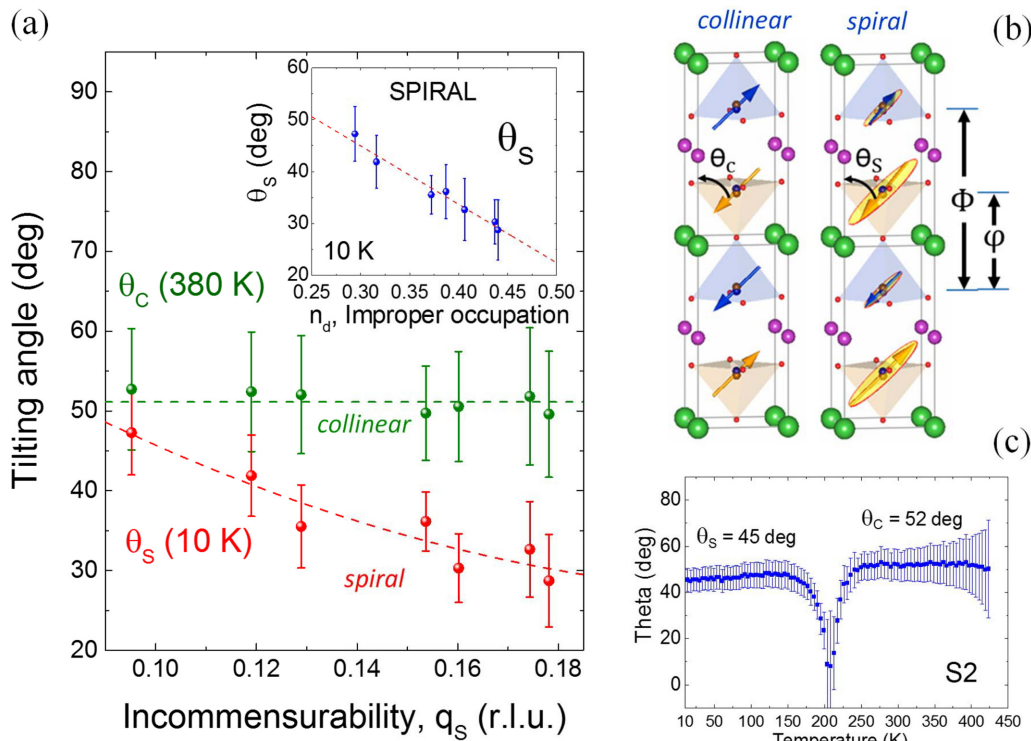
FIG. 8. Influence of the improper Fe/Cu occupation (n_d, chemical disorder) in YBCFO on the inclination angle θ_S of the spiral rotation plane determined at 10 K (red symbols). Flat dependence of the inclination θ_C of the collinear spins in the CM phase (at 380 K) is also shown (black symbols). Dashed lines are lineal fits to the experimental points (data from Table II). In the inset these tilting angles are plotted vs the ICM modulation q_S of the samples. Notice the linear dependence of θ_S (n_d). (b) Projection showing the evolution of the tilting of the rotation plane by increasing the improper Fe/Cu occupation (n_d). (c) Example of the T dependence of the inclination angle of the collinear spins ($T_S < T < T_{N1}$) and of the spiral rotation plane ($T < T_S$) (sample S2; the slope $d\theta_S/dT \approx 0.025$ °/K).

The progressive reorientation of the rotation plane of the spins is schematically illustrated in Fig. 9(b). Regarding samples S1 and S7, the most distant in terms of disorder, there is between them a reorientation $\Delta\theta_S$ of the spiral plane of $\approx -20°$. In Fig. 9(a) the arrows represent the average ordered moment in each pyramid according to the values gathered in Table II. The blue (brown) color applies to CuO_5 (FeO_5) pyramids. The degree of Fe/Cu disorder in each pyramid is represented by mixing both colors according to the improper occupation n_d in that site. For that reason the colors of the two pyramids in the cell become increasingly similar in Fig. 9(a), and finally end up being almost indistinguishable from each other in the most disordered samples [$n_d \sim 0.44(4)$ in sample S7].

D. The magnetic "phase-separation" region: Beyond the triple point in YBaCuFeO₅

A magnetic triple point was initially proposed for $YBa_{1-x}Sr_x Cu Fe O_5$ samples quenched into liquid nitrogen in Ref. [11]. Here we have shown that the convergence of T_{N1} and T_S, which imposes the limit for the highest spiral temperature, can be attained in samples with identical composition $YBaCuFeO_5$ without the need to increase the number of dissimilar divalent cations in the A site of the structure. A noteworthy experimental conclusion is that in bulk samples the triple point represents a critical end point for the incommensurate spiral phase. The stability of this modulated order cannot overcome the stability of the collinear order. At least

in the absence of external perturbations, the spiral order by disorder mechanism requires and cannot avoid a commensurate collinear phase preceding the spiral incommensurate magnetic order. This observation confirms that the orientationally aligned frustrated bonds in YBCFO cannot generate a paramagnetic–spiral phase boundary of finite size. The energy terms deciding the magnetic configuration to adopt at a given temperature below the Néel point were analyzed in Refs. [7,9,12,13]. Moreover, given the concurrence of disordered and ordered spin configurations, the latter undergoing a transition between spatially uniform (commensurate) and spatially modulated (incommensurate) magnetic orders, the triple point in YBCFO seems a good candidate for a possible Lifshitz multicritical point [31–33].

In addition, notice that the phase diagram in Fig. 7(a) is not strictly equivalent to that reported by Shang *et al.* in the vicinity of the triple point [11]. In that one the driving force approaching the triple point ($YBa_{1-x}Sr_x Cu Fe O_5$ samples with increasing Sr content) are structural effects produced by A-site cationic substitutions with little or no change in the Fe/Cu disorder. For that reason the slope dT_S/dq_S is clearly dissimilar when comparing the $YBaCuFeO_5$ (B-site disorder) and the $YBa_{1-x}Sr_x Cu Fe O_5$ (Sr content) series of samples. In the phase diagram of Fig. 7(a) composition does not change. When comparing the ICM transition temperatures, the maximum Fe/Cu disorder of YBCFO in Ref. [11] is significantly lower than in our sample S4 (being $T_S \approx 310$ K in Ref. [11], its disorder should be between the present samples S3 and S4).
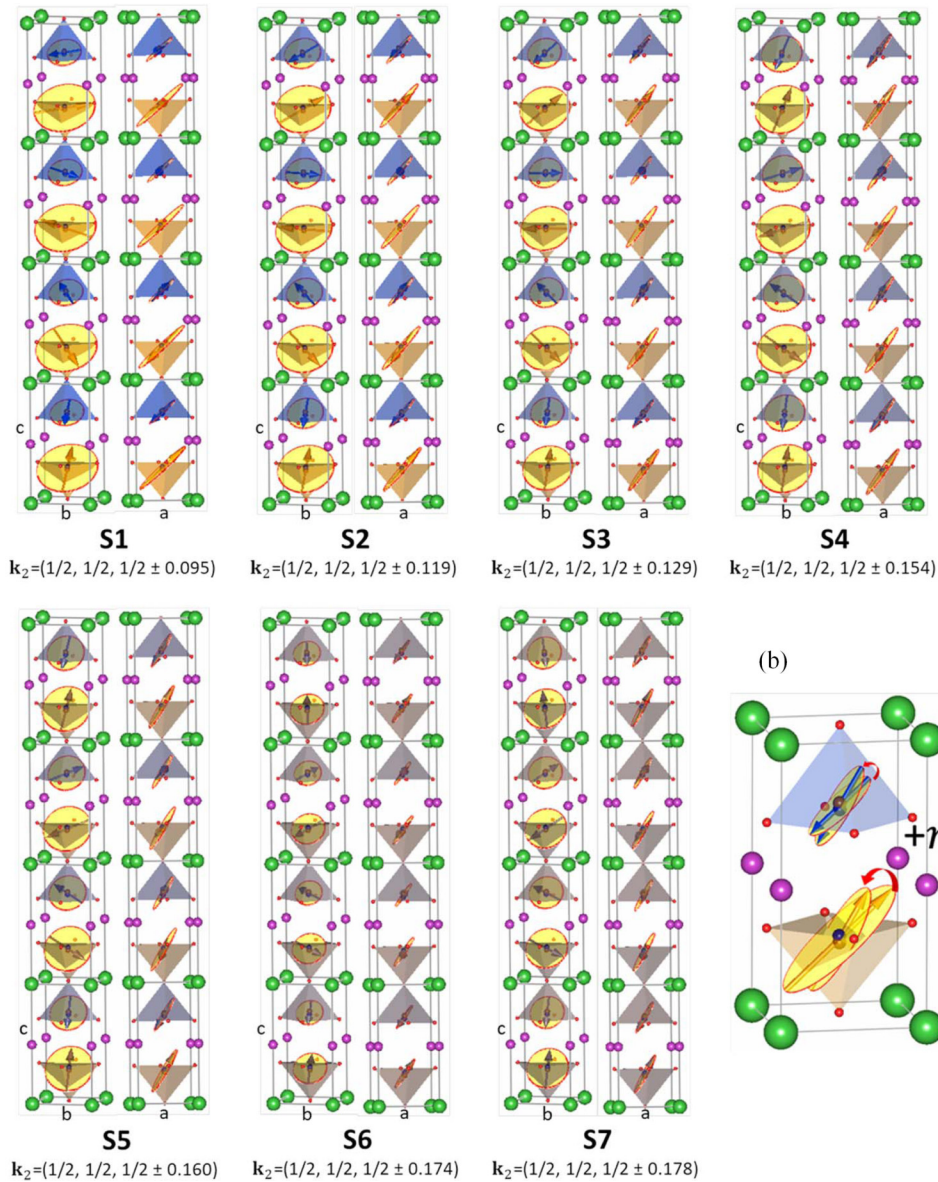
FIG. 9. (a) Two projections of the refined circular spiral order at 10 K in YBCFO samples with increasing Fe/Cu disorder (model 2 described in Table II). Incommensurate magnetic propagation vector determined in each sample is indicated. (b) Sketch of the evolution of the orientation of the spiral rotation plane when increasing disorder (n_d). For clarity, the average magnetic moment is depicted in each pyramid. Colors of the moments and pyramids reflect the fraction of Cu/Fe ions (blue/brown) at each site.

The driving force along the x axis in the phase diagram of Fig. 7(a) is strictly the Fe/Cu chemical disorder, which extends T_S up to ≈ 366 K (sample S7). On the other hand, from the magnetic phase diagram [Fig. 7(a)] we can also identify the critical values at the intersection (triple) point. For this one can combine the linear relationships listed in Table III for the pairs T_{N1}-q_S and T_{N2}-q_S, and imposing $T_{N1} = T_{N2}$ one gets $q_s^c = 0.186(13)$ r.l.u. and $T_s^c = 407(16)$ K ($T_{N1}^c = T_s^c$). Here, q_s^c and T_s^c stand for the "extrapolated" critical values at the triple point. In the same way, the corresponding critical disorder, $n_d^c = 0.47(3)$, is found below but very close to the maximum possible disorder $n_d = 0.5$.

What happens then when in this structure the Fe/Cu disorder acquires values greater than n_d^c ? The answer is that the system enters in another regime that we have named the "phase-separated" region [see Fig. 7(a)]. Ideally, the phase-separated region corresponds to samples with a degree of Fe/Cu disorder within the interval $n_d^c < n_d < 0.5$, and it is characterized by the presence of magnetic phase segregation. We expect this region to be characterized by the competition of emergent collinear AF3 and declining AF1 regions, whereas spiral order rapidly vanishes [11]. The AF3 configuration is favored in front of the AF1 and AF2 ones when the competition between FM and AFM
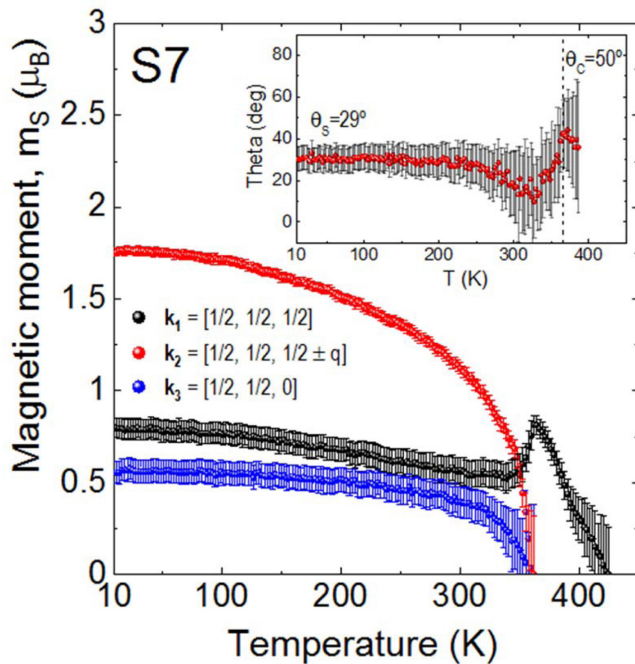
FIG. 10. Phase-separation regime. Sample S7 [highest disorder level, $n_d = 0.44(4)$]. T dependence of the ordered magnetic moments (m_S, averaged over the total sample volume) associated with the coexisting magnetic phases in the phase-separation regime. Inset: Evolution of the inclination angle θ of the magnetic easy axis in the collinear ($T_S < T < T_{N1}$) and spiral orders ($T < T_S$).

lows us to extract several conclusions on the phase separation beyond the triple point. (i) The first is that when disorder exceeds n_d^c, a multidomain magnetic texture is favored where the coexisting magnetic orders ($\mathbf{k}_1$, $\mathbf{k}_2$, and $\mathbf{k}_3$) share $(k_x, k_y) = (1/2, 1/2)$ but differ in their translational symmetry parallel to the improper bonds along the c axis ($k_z = 0$, $1/2 \pm q$, and $1/2$). (ii) Second, the collinear $\mathbf{k}_1 = (1/2, 1/2, 1/2)$ magnetic domains start to develop prior to the ICM spiral order in all the cases. Moreover, when cooling from the paramagnetic state, $\mathbf{k}_1$ always emerges before $\mathbf{k}_3$-type domains. (iii) Third, this additional CM magnetic domains characteristic of the phase-separation regime [$\mathbf{k}_3 = (1/2, 1/2, 0)$] develops simultaneously to the ICM $\mathbf{k}_2 = (1/2, 1/2, 1/2 \pm q)$ order. As an example, we show in Fig. 10 the simultaneous appearing of $(1/2, 1/2, 0)$ $\mathbf{k}_3$ and spiral $\mathbf{k}_2$ magnetic intensity in the sample S7, coinciding with the partial collapse of the $(1/2, 1/2, 1/2)$ order. This third observation can be interpreted as a consequence of the limitations anticipated in the model. The required conditions to stabilize the spiral were analyzed in Refs. [12,13] and some concern the distribution of improper Fe-Fe bonds in the structure. In particular, the spiral order is not favored in those regions where neighbouring Fe-Fe bonds are closer along the c axis (the orientation of the impurity bonds) than within the bilayer (*ab* plane). Predictably, when chemical disorder is too high, unsatisfied conditions in certain parts of the volume would explain the appearance of additional competing translational orders and the phase-separation regime.

VI. CONCLUSION

Frustrated magnets displaying spiral magnetic orders (conical screw, cycloidal, helimagnetic, etc.) at ambient temperatures are intrinsically rare. In nongeometrically frustrated structures (such as YBCFO) this typically requires competing nearest-neighbors and next-nearest-neighbors interactions of similar strength and both strong, which is highly unlikely. This bottleneck can be avoided if frustration is generated by chemical disorder. The exceptional stability of the spiral magnetic order in the layered perovskite structure investigated here entails a nonconventional mechanism that, as proposed by Scaramucci and co-workers, relies on the presence of random strongly frustrating antiferromagnetic bonds introduced along a single crystallographic direction [12,13]. As a credible realization of this model, we have methodically investigated and described the influence of tuning frustration in YBCFO through *B*-site cation disorder, covering practically the full interval between total order and random disorder. Our understanding of these layered perovskites is disclosing a radical mechanism for stabilization of cycloidal (spiral) orders in which frustration has no geometrical or electronic origins but it is essentially based on chemical disorder. The quantitative and thorough description of the interplay between disorder (frustration) and the magnetic and structural features illustrates in this reference composition the avenue spiral order by disorder to supply noncollinear functional magnets at normal working temperatures. It can help to define or inspire design strategies in these and other anisotropic functional magnets able to adopt phases with magnetic chirality at high temperatures.

tendencies inside the bipyramids gets unbalanced by an excessive number of strongly AFM Fe-Fe bipyramids. In our most disordered samples (real, not ideal, materials) the phase coexistence includes the magnetic propagation vectors $\mathbf{k}_1 = (1/2, 1/2, 1/2)$, $\mathbf{k}_2 = (1/2, 1/2, 1/2 \pm q)$, and $\mathbf{k}_3 = (1/2, 1/2, 0)$. Here, we want to stress the fact that in real samples (powders or crystals), beyond the average disorder n_d, local fluctuations in the distribution of Fe/Cu atoms very likely play also a role. Namely, the variance $\sigma^2[n_d]$ and its spatial distribution can also favor magnetic phase separation. On one hand, inhomogeneous disorder (very dependent on the preparation) explains the possibility of preparing samples with the same apparent magnetic modulation and transition temperature but different residual amount of collinear phase at low temperature [as occurs in our sample S3, Fig. 6(a)]. On the other hand, another consequence of certain inhomogeneous disorder is that it smears out the boundary separating the spiral and the phase-separated regions [as exposed in Fig. 7(a)]. So, a certain degree of inhomogeneous disorder can explain the presence of the three magnetic phases (the emergent collinear AF3 [$\mathbf{k}_3$], the AF1 one [$\mathbf{k}_1$], and also the spiral) in the two most disordered YBCFO samples (S6 and S7). However, it is important to stress that spiral order with q_S larger than $q_s^c \approx 0.18$ r.l.u. has not been observed.

In Fig. 6(a) the coexisting magnetic phases characteristic of the phase-separation region are apparent in samples S6 and S7. To get a closer view of this region of disorder, the evolution of the representative magnetic intensities for sample S7, the less ordered sample, is displayed in Fig. 10. This figure al-

[1] S. Seki, X. Z. Yu, S. Ishiwata, and Y. Tokura, Observation of skyrmions in a multiferroic material, Science **336**, 198 (2012).

[2] G. Lawes, B. Melot, K. Page, C. Ederer, M. A. Hayward, Th. Proffen, and R. Seshadri, Dielectric anomalies and spiral magnetic order in $CoCr_2O_4$, Phys. Rev. B **74**, 024413 (2006).

[3] S. Dong, J. M. Liu, S. W. Cheong, and Z. Ren, Multiferroic materials and magnetoelectric physics: Symmetry, entanglement, excitation, and topology, Adv. Phys. **64**, 519 (2015).

[4] E. Bousquet and A. Cano, Non-collinear magnetism in multiferroic perovskites, J. Phys.: Condens. Matter **28**, 123001 (2016).

[5] V. Caignaert, I. Mirebeau, F. Bourée, N. Nguyen, A. Ducouret, J. M. Greneche, and B. Raveau, Crystal and magnetic structure of $YBaCuFeO_5$, J. Solid State Chem. **114**, 24 (1995).

[6] B. Kundys, A. Maignan, and C. Simon, Multiferroicity with high-T_C in ceramics of the $YBaCuFeO_5$ ordered perovskite, Appl. Phys. Lett. **94**, 072506 (2009).

[7] M. Morin, A. Scaramucci, M. Bartkowiak, E. Pomjakushina, G. Deng, D. Sheptyakov, L. Keller, J. Rodriguez-Carvajal, N. A. Spaldin, M. Kenzelmann, K. Conder, and M. Medarde, Incommensurate magnetic structure, Fe/Cu chemical disorder, and magnetic interactions in the high-temperature multiferroic $YBaCuFeO_5$, Phys. Rev. B **91**, 064408 (2015).

[8] Y. Kawamura, T. Kai, E. Satomi, Y. Yasui, Y. Kobayashi, M. Sato, and K. Kakurai, High-temperature multiferroic state of $RBaCuFeO_5$ ($R = Y$, Lu, and Tm), J. Phys. Soc. Jpn. **79**, 073705 (2010).

[9] M. Morin, E. Canévet, A. Raynaud, M. Bartkowiak, D. Sheptyakov, V. Ban, M. Kenzelmann, E. Pomjakushina, K. Conder, and M. Medarde, Tuning magnetic spirals beyond room temperature with chemical disorder, Nat. Commun. **7**, 13758 (2016).

[10] Y. C. Lai *et al.*, Magnetic ordering and dielectric relaxation in the double perovskite $YBaCuFeO_5$, J. Phys.: Condens. Matter **29**, 145801 (2017).

[11] T. Shang, E. Canévet, M. Morin, D. Sheptyakov, M. Teresa Fernández-Díaz, E. Pomjakushina, M. Medarde, M. T. Fernández-Díaz, E. Pomjakushina, and M. Medarde, Design of magnetic spirals in layered perovskites: Extending the stability range far beyond room temperature, Sci. Adv. **4**, eaau6386 (2018).

[12] A. Scaramucci, H. Shinaoka, M. V. Mostovoy, M. Müller, C. Mudry, M. Troyer, and N. A. Spaldin, Multiferroic Magnetic Spirals Induced by Random Magnetic Exchanges, Phys. Rev. X **8**, 011005 (2018).

[13] A. Scaramucci, H. Shinaoka, M. V. Mostovoy, R. Lin, C. Mudry, and M. Müller, Spiral order from orientationally correlated random bonds in classical XY models, Phys. Rev. Res. **2**, 013273 (2020).

[14] N. Momozawa, Y. Yamaguchi, and H. Takei, Magnetic structure of $(Ba_{1-x}Sr_x)_2Zn_2Fe_{12}O_{22}$ ($x = 0$–1.0), J. Phys. Soc. Jpn. **54**, 771 (1985).

[15] S. Utsumi, D. Yoshiba, and N. Momozawa, Superexchange interactions of $(Ba_{1-x}Sr_x)_2Zn_2Fe_{12}O_{22}$ system studied by neutron diffraction, J. Phys. Soc. Jpn. **76**, 034704 (2007).

[16] D. E. Cox, W. J. Takei, and G. Shireen, A magnetic and neutron diffraction study of the Cr_2O_3-Fe_2O_3 system, J. Phys. Chem. Solids **24**, 405 (1963).

[17] F. Faith, R. Boer, F. Gil-Ortiz, C. Popescu, O. Allora, I. Peral, D. Full, J. Benach, and J. Juanhuix, The crystallography stations at the Alba synchrotron, Eur. Phys. J. Plus **130**, 160 (2015).

[18] J. Rodríguez-Carvajal, Recent advances in magnetic structure determination by neutron powder diffraction, Phys. B: Condens. Matter **192**, 55 (1993).

[19] M. I. Aroyo, J. M. Perez-Mato, C. Capillas, E. Kroumova, S. Ivantchev, and G. Madariaga, Bilbao Crystallographic Server: I. Databases and crystallographic computing programs, Z. Kristallogr. **221**, 15 (2006).

[20] J. M. Perez-Mato, S. V. Gallego, E. S. Tasci, L. Elcoro, G. de la Flor, and M. I. Aroyo, Symmetry-based computational tools for magnetic crystallography, Annu. Rev. Mater. Res. **45**, 217 (2015).

[21] M. I. Aroyo, A. Kirov, C. Capillas, J. M. Perez-Mato, and H. Wondratschek, Bilbao Crystallographic Server. II. Representations of crystallographic point groups and space groups, Acta Crystallogr., Sect. A: Found. Crystallogr. **62**, 115 (2006).

[22] B. J. Campbell, H. T. Stokes, D. E. Tanner, and D. M. Hatch, ISODISPLACE: A Web-based tool for exploring structural distortions, J. Appl. Crystallogr. **39**, 607 (2006).

[23] K. Momma and F. Izumi, VESTA 3 for three-dimensional visualization of crystal, volumetric and morphology data, J. Appl. Crystallogr. **44**, 1272 (2011).

[24] W. C. Liu, Y. Z. Zheng, Y. C. Chih, Y. C. Lai, Y. W. Tsai, Y. Z. Zheng, C. H. Du, F. C. Chou, Y. L. Soo, and S. L. Chang, *X-Ray* multi-beam resonant diffraction analysis of crystal symmetry for layered perovskite $YBaCuFeO_5$, J. Appl. Crystallogr. **49**, 1721 (2016).

[25] See Supplemental Material at http://link.aps.org/supplemental/10.1103/PhysRevResearch.4.043188 for more details about synchrotron x-ray and neutron pattern refinements of YBCFO samples; evolution of some structural details, cation positions, interatomic distances, and the refined magnetic structures increasing B-site disorder.

[26] X. Zhang, A. Romaguera, O. Fabelo, F. Fauth, J. Herrero-Martín, and J. L. García-Muñoz, Tuning the tilting of the spiral plane by Mn doping in YBaCuFeO$_5$ multiferroic, Acta Mater. **206**, 116608 (2021).

[27] In this system the structural characterization (including cation occupancies) using SXRD has several advantages. One is the lack of magnetic intensity, which is present up to very high temperatures (T_{N1}) in the neutron-diffraction patterns. Another is that it overcomes the very similar neutron scattering lengths for Cu and Fe: 9.45 fm for Fe and 7.72 fm for Cu.

[28] X. Zhang, A. Romaguera, F. Sandiumenge, O. Fabelo, J. Blasco, J. Herrero-Martín, and J. L. García-Muñoz, Magnetic properties of a highly ordered single crystal of the layered perovskite YBaCuFe$_{0.95}$Mn$_{0.05}$O$_5$, J. Magn. Magn. Mater. **551**, 169165 (2022).

[29] Y.-S. Song, L. Q. Yan, B. Lee, S. H. Chun, K. H. Kim, S. B. Kim, A. Nogami, T. Katsufuji, J. Schefer, and J.-H. Chung, Chemical doping-induced flop of ferroelectric polarization in multiferroic Mn$_{0.9}$Co$_{0.1}$WO$_4$, Phys. Rev. B **82**, 214418 (2010).

[30] In Fig. 1 [q_S vs n_d] we used a linear regression fit for the sake of simplicity.

[31] R. M. Hornreich, M. Luban, and S. Shtrikman, Critical Behavior at the Onset of K→-Space Instability on the Λ Line, Phys. Rev. Lett. **35**, 1678 (1975).

[32] R. M. Hornreich, The Lifshitz point: Phase diagrams and critical behavior, J. Magn. Magn. Mater. **15**, 387 (1980).

[33] H. C. Chauhan, B. Kumar, J. K. Tiwari, and S. Ghosh, Multiple phases with a tricritical point and a Lifshitz point in the skyrmion host Cu$_2$OSeO$_3$, Phys. Rev. B **100**, 165143 (2019).